Spectral Graph Coarsening Using Inner Product Preservation and the Grassmann Manifold

Ido Cohen
Electrical and Computer Engineering
Technion–Israel Institute of Technology
sidoc@campus.technion.ac.il

Ronen Talmon
Electrical and Computer Engineering
Technion–Israel Institute of Technology
ronen@ee.technion.ac.il

Abstract

We propose a novel functorial graph coarsening method that preserves inner products between node features, a property often overlooked by existing approaches focusing primarily on structural fidelity. By treating node features as functions on the graph and preserving their inner products, our method retains both structural and feature relationships, facilitating substantial benefits for downstream tasks. To formalize this, we introduce the Inner Product Error (IPE), which quantifies how the inner products between node features are preserved. Leveraging the underlying geometry of the problem on the Grassmann manifold, we formulate an optimization objective that minimizes the IPE, also for unseen smooth functions. We show that minimizing the IPE improves standard coarsening metrics, and illustrate our method's properties through visual examples that highlight its clustering ability. Empirical results on benchmarks for graph coarsening and node classification show that our approach outperforms existing state-of-the-art methods.

1 Introduction

Graph-structured data has become ubiquitous in a wide range of domains, including social networks [1], biological systems [2], and recommendation systems [3], due to its ability to model complex relationships and interactions. With the exponential increase in data availability, the size of graphs in many applications has also grown significantly. This surge in graph size presents major challenges, as traditional and even advanced graph processing techniques often become computationally infeasible or excessively time-consuming when applied to large-scale graphs. To address these issues, graph reduction techniques are developed with the aim of simplifying large graphs while retaining key structural features, thereby enhancing computational efficiency. There are three main strategies for graph reduction [4]: graph sparsification, graph condensation, and graph coarsening.

Graph sparsification [5, 6] reduces graph size by selectively removing edges and nodes while maintaining overall structural properties. However, there is a limit to how much a graph can be sparsified without compromising its integrity. Graph condensation methods [7, 8] aim to reduce graph size by generating a smaller, synthetic graph that replicates the performance of the original graph on specific tasks, such as training a Graph Neural Network (GNN). Although condensation significantly lowers computational costs, it may not retain a clear structural interpretation, making it difficult to understand how or why certain nodes or edges are represented in the reduced version.

In contrast, graph coarsening [9] is a traditional approach that reduces graph size by grouping similar nodes into super-nodes, aiming to approximate the original structure. These methods typically seek to preserve key structural properties such as spectral characteristics [10], connectivity [11], and community structure [12, 13]. Most existing coarsening methods focus primarily on structure and often overlook node features, which play a critical role in many graph learning tasks. These methods typically operate solely on the graph topology, neglecting the rich information encoded in the node

39th Conference on Neural Information Processing Systems (NeurIPS 2025).

features. Recently, the Featured Graph Coarsening (FGC) method was proposed to address this limitation by incorporating node features into the coarsening process [14]. FGC emphasizes the reconstruction of the node features after coarsening and promotes smoothness in the coarsened graph as part of its optimization objective. However, since FGC focuses on preserving the individual characteristics of the node features, it does not fully exploit their mutual relationships, which may encode valuable information.

In this work, we propose a new approach to graph coarsening from a functorial perspective. We treat node features as functions, or signals, defined on the graph, focusing on preserving the relationships between these functions by maintaining their inner products during coarsening. Our method introduces a new coarsening metric, the Inner Product Error (IPE), which measures how the inner products between graph signals are preserved. We postulate that minimizing IPE ensures that the coarsened graph retains structural consistency and node feature relationships crucial for graph learning tasks. We exploit the geometry of the problem by recognizing that both the coarsening operator and the matrix spanning the node features (under a smoothness assumption) can be viewed as points on the Grassmann manifold. Leveraging the properties of the Grassmann manifold, we extend IPE minimization beyond observed node features, enabling our method to generalize to unseen features that satisfy the smoothness assumption. This approach is formulated as an optimization problem, and we compute the coarsening operator using gradient descent. Additionally, we theoretically show that minimizing our proposed approach leads to improvements in common graph coarsening metrics.

To demonstrate the effectiveness of our method, we present visual and empirical results showing that, while our method focuses on the functional relationships between node features, it also captures the global structure of the graph. We validate its performance through extensive experiments on multiple graph coarsening and node classification benchmarks, where our method consistently outperforms state-of-the-art coarsening methods, demonstrating its practical utility.

2 Background

Grassman manifold The set of $n \times k$ matrices whose columns are orthonormal vectors forms a Riemannian manifold called the Stiefel manifold [15] defined by,

$$\mathrm{St}(n,k) := \{\boldsymbol{U} \in \mathbb{R}^{n\times k} | \boldsymbol{U}^T\boldsymbol{U} = \boldsymbol{I}_{k\times k}\}. \tag{1}$$

where $\boldsymbol{I}_{k\times k}$ is a rank-k identity matrix. The Grassmann manifold $\mathrm{Gr}(n,k)$ is a quotient manifold representing the set of k-dimensional subspaces of the Euclidean space $\mathbb{R}^n$. Two points on the Stiefel manifold that span the same subspace represent the same point on the Grassmann manifold [16, 17]. In general, a point on $\mathrm{Gr}(n,k)$ is represented by an equivalence class

$$[\boldsymbol{U}] = \{\boldsymbol{U}\boldsymbol{O} : \boldsymbol{O} \in \mathcal{SO}(k)\}, \tag{2}$$

where $\boldsymbol{U} \in \mathrm{St}(n,k)$, and $\mathcal{SO}(k)$ are all $k \times k$ rotation matrices (also known as the special orthogonal group), such that any $\boldsymbol{O} \in \mathcal{SO}(k)$ satisfies $\boldsymbol{O}\boldsymbol{O}^T = \boldsymbol{O}^T\boldsymbol{O} = \boldsymbol{I}_{k\times k}$. The principal angles between two subspaces $\boldsymbol{U}_1$ and $\boldsymbol{U}_2$ are the angles that measure the smallest angular separation between basis vectors in one subspace and basis vectors in the other subspace. We denote them by $\boldsymbol{\theta} = [\theta^{(1)}, \theta^{(2)}, \ldots, \theta^{(k)}]$. Given two subspaces $\boldsymbol{U}_1$ and $\boldsymbol{U}_2$ on the Grassmann manifold $\mathrm{Gr}(n,k)$, the cosine of the principal angles between them can be computed using the SVD decomposition of $\boldsymbol{U}_1^T\boldsymbol{U}_2 = \boldsymbol{A}\boldsymbol{\Theta}\boldsymbol{B}^T$, where the singular values on the diagonal of $\boldsymbol{\Theta}$ are $[\cos(\theta^{(1)}), \cos(\theta^{(2)}), \ldots, \cos(\theta^{(k)})]$.

The geodesic similarity on the Grassmann manifold is defined using the principal angles between subspaces [17]. The authors in [18] showed that this geodesic similarity can be computed by,

$$Gr(\boldsymbol{U}_1, \boldsymbol{U}_2) = \sum_{i=1}^{k} \cos^2(\theta^{(i)}) = tr(\boldsymbol{U}_1\boldsymbol{U}_1^T\boldsymbol{U}_2\boldsymbol{U}_2^T). \tag{3}$$

Graph coarsening A graph with node features is denoted by the quadruplet $\mathcal{G} = (\mathcal{V}, \mathcal{E}, \boldsymbol{W}, \boldsymbol{X})$, where $\mathcal{V}$ is a set of n vertices, $\mathcal{E}$ is a set of edges, $\boldsymbol{W} \in \mathbb{R}^{n\times n}$ is a weighted adjacency matrix, and $\boldsymbol{X} \in \mathbb{R}^{n\times p}$ is a node features matrix such that each row specifies the values of the p features for each node. Each node feature, represented as a column of $\boldsymbol{X}$, can also be considered as a graph signal $\boldsymbol{x} \in \mathbb{R}^n$, assigning a real value to each vertex, namely, $\boldsymbol{x} : \mathcal{V} \to \mathbb{R}$. The graph Laplacian matrix $\boldsymbol{L}$ is

defined by $\boldsymbol{L} = \boldsymbol{D} - \boldsymbol{W}$, where $\boldsymbol{D} = \text{diag}(\boldsymbol{W}\mathbf{1})$ is the diagonal degree matrix. We define the inner product between two graph signals $\boldsymbol{x}, \boldsymbol{y} \in \mathbb{R}^n$ with respect to the graph $\mathcal{G}$ by:

$$\langle \boldsymbol{x}, \boldsymbol{y} \rangle_L = \boldsymbol{x}^T \boldsymbol{L}\boldsymbol{y} = \sum_{(i,j)\in E} w_{ij}(\boldsymbol{x}(i) - \boldsymbol{x}(j))(\boldsymbol{y}(i) - \boldsymbol{y}(j)), \tag{4}$$

where w_{ij} are edge weights, and $\boldsymbol{x}(i), \boldsymbol{y}(i)$ are the values of the features at node i. Since $\boldsymbol{L}$ is a positive semi-definite matrix, $\boldsymbol{x}^\top \boldsymbol{L}\boldsymbol{x}$ induces a semi-norm and defines an inner product on the subspace of $\mathbb{R}^n$ orthogonal to the constant vector $\mathbf{1}$, as discussed in Von Luxburg [19]. We denote the graph Laplacian eigen decomposition by $\boldsymbol{L} = \boldsymbol{U}\boldsymbol{\Lambda}\boldsymbol{U}^T$, where the columns of $\boldsymbol{U}$ are the eigenvectors of $\boldsymbol{L}$, and $\boldsymbol{\Lambda}$ is a diagonal matrix consisting of its corresponding eigenvalues.

Given a graph $\mathcal{G} = (\mathcal{V}, \mathcal{E}, \boldsymbol{W}, \boldsymbol{X})$ with n nodes, the goal of graph coarsening is to construct a coarsened graph $\mathcal{G}_c = (\mathcal{V}_c, \mathcal{E}_c, \boldsymbol{W}_c, \boldsymbol{X}_c)$ with $k \ll n$ nodes, while preserving the main structural properties of $\mathcal{G}$, thereby simplifying subsequent analysis and computations. The coarsening procedure is defined through a linear mapping $\pi : \mathcal{V} \to \mathcal{V}_c$ that maps nodes in $\mathcal{G}$ to nodes in $\mathcal{G}_c$, termed 'super-nodes'. This linear mapping is defined by the coarsening matrix $\boldsymbol{P} \in \mathbb{R}_+^{k\times n}$, such that $\boldsymbol{X}_c = \boldsymbol{P}\boldsymbol{X}$. Each non-zero entry of $\boldsymbol{P}$ indicates a mapping from a node in $\mathcal{G}$ to a super-node in $\mathcal{G}_c$, i.e., if and only if the j-th node in $\mathcal{G}$ is mapped to the i-th super-node of $\mathcal{G}_c$, then $\boldsymbol{P}_{i,j} > 0$. Let $\boldsymbol{L} \in \mathbb{R}^{n\times n}$ and $\boldsymbol{L}_c \in \mathbb{R}^{k\times k}$ be the respective Laplacian matrices of $\mathcal{G}$ and $\mathcal{G}_c$, and let $\boldsymbol{L}_l \in \mathbb{R}^{n\times n}$ and $\boldsymbol{X}_l \in \mathbb{R}^{n\times p}$ be the lifted Laplacian and feature matrices, i.e., the reconstructed full graph matrices after the coarsening procedure. The relationships between the coarse graph Laplacian and features and the original graph Laplacian and features are [20]:

$$\boldsymbol{L}_c = \boldsymbol{C}^\top \boldsymbol{L}\boldsymbol{C}, \qquad \boldsymbol{X}_c = \boldsymbol{P}\boldsymbol{X} \tag{5}$$

$$\boldsymbol{L}_l = \boldsymbol{P}^\top \boldsymbol{L}_c \boldsymbol{P}, \qquad \boldsymbol{X}_l = \boldsymbol{C}\boldsymbol{X}_c \tag{6}$$

where $\boldsymbol{C} \in \mathbb{R}_+^{n\times k}$ is the pseudo-inverse of $\boldsymbol{P}$, i.e., $\boldsymbol{C} = \boldsymbol{P}^\dagger$. The non-zero entries of $\boldsymbol{C}$ also imply a node mapping from $\mathcal{G}$ to $\mathcal{G}_c$, such that $\boldsymbol{C}_{i,j} > 0$ if the i-th node of $\mathcal{G}$ is mapped to the j-th super-node of $\mathcal{G}_c$. We note that the matrix $\boldsymbol{C}$ belongs to the following set:

$$\begin{aligned} \mathcal{C} = \{\boldsymbol{C} \geq 0 | \langle \boldsymbol{C}_{:,i}, \boldsymbol{C}_{:,j} \rangle = 0 \quad \forall i \neq j, \\ \langle \boldsymbol{C}_{:,i}, \boldsymbol{C}_{:,i} \rangle = d_i, \|\boldsymbol{C}_{:,i}\|_0 \geq 1, \|\boldsymbol{C}_{i,:}\|_0 = 1\} \end{aligned} \tag{7}$$

where $\boldsymbol{C}_{:,i}$ is the i-th orthogonal column of $\boldsymbol{C}$, $\boldsymbol{C}_{i,:}$ is the i-th row of $\boldsymbol{C}$, $\langle \cdot, \cdot \rangle$ is the standard inner product, and d_i is some positive number. Since the columns of a valid coarsening matrix $\boldsymbol{C}$ are orthogonal, it can also be viewed as a point on the Grassmann manifold $\text{Gr}(n, k)$.

Numerous evaluation metrics exist for graph coarsening, each assessing how well specific graph properties are preserved during reduction. Next, we review the main ones.

Definition 2.1 (Relative Eigen Error (REE) [10]) *The REE is defined as* $REE = \frac{1}{k}\sum_{i=1}^{k} \frac{\lambda_{c,i} - \lambda_i}{\lambda_i}$, *where* λ_i *and* $\lambda_{c,i}$ *are the* k *dominant eigenvalues of the original graph Laplacian matrix* $\boldsymbol{L}$ *and the coarsened graph Laplacian matrix* $\boldsymbol{L}_c$, *respectively.*

Definition 2.2 (Reconstruction Error (RE) [21]) *The RE between the original graph Laplacian* $\boldsymbol{L}$ *and the lifted graph Laplacian* $\boldsymbol{L}_l$ *is defined by* $RE = \|\boldsymbol{L} - \boldsymbol{L}_l\|_F^2$.

The REE and RE are coarsening metrics independent of the graphs' node features. The REE measures the spectral similarity between graphs and how global properties such as important edges are preserved, while the RE quantifies how local information is preserved during coarsening.

Definition 2.3 (Hyperbolic Error (HE) [22]) *The HE between the original Laplacian matrix* $\boldsymbol{L}$ *and lifted Laplacian matrix* $\boldsymbol{L}_l$ *is defined as* $HE = arccosh\left(1 + \frac{\|(\boldsymbol{L}-\boldsymbol{L}_l)\boldsymbol{X}\|_F^2 \|\boldsymbol{X}\|_F^2}{2tr(\boldsymbol{X}^T\boldsymbol{L}\boldsymbol{X})tr(\boldsymbol{X}^T\boldsymbol{L}_l\boldsymbol{X})}\right)$, *where* $\boldsymbol{X}$ *is the node features matrix of the original graph.*

Definition 2.4 (Dirichlet Energy Error (DEE)) *The Dirichlet Energy (DE) of a graph is defined by* $DE = tr(\boldsymbol{X}^\top \boldsymbol{L}\boldsymbol{X})$, *where* $\boldsymbol{L}$ *denotes the graph Laplacian and* $\boldsymbol{X}$ *denotes the node feature matrix of the graph [23]. We define the DEE between the original graph* $\mathcal{G}$ *and its coarsened version* $\mathcal{G}_c$ *as* $DEE = \left|\log\left(\frac{DE_{\mathcal{G}}}{DE_{\mathcal{G}_c}}\right)\right|$, *where* $DE_{\mathcal{G}}$ *and* $DE_{\mathcal{G}_c}$ *are the DE of the original and coarsened graphs.*

The HE and DEE are coarsening measures that consider the node features. The HE measures distortion in the geometric structure of the data in hyperbolic space. This is useful when the graph

has a hierarchical structure (e.g., trees), as hyperbolic spaces are suited for representing such data. The DE measures the smoothness of the node features on a graph; lower DE values suggest that the node features are closely aligned with the graph structure. Consequently, we define the DEE which quantifies the extent to which the intrinsic graph structure in the node features is preserved during the coarsening process. We note that the authors in Kumar et al. [14] suggest minimizing the DE of the coarsened graph as part of their graph coarsening optimization objective.

3 Proposed method

Our method adopts a functorial perspective for graph coarsening, focusing on maintaining the relationships between different functions defined on the graph. Specifically, it aims to preserve the inner products between functions defined on the graph. To achieve this, we first introduce the following new graph coarsening metric that quantifies how the inner products between given graph signals (i.e., node features) are preserved during the coarsening process.

Definition 3.1 (Inner Product Error (IPE)) *Let $\boldsymbol{L}$ and $\boldsymbol{X}$ be the original graph Laplacian and node features matrix, and let $\boldsymbol{L}_c$ and $\boldsymbol{X}_c$ be their respective coarsened graph Laplacian and features matrix. The Inner Product Error (IPE) is defined by IPE $= \|\boldsymbol{X}^\top \boldsymbol{L}\boldsymbol{X} - \boldsymbol{X}_c^\top \boldsymbol{L}_c \boldsymbol{X}_c\|_F^2$.*

The motivation for this approach is based on the following:

Proposition 3.2 *Let $\boldsymbol{L}$ and $\boldsymbol{L}_c$ be the graph Laplacians of a graph $\mathcal{G}$ and its coarsened graph $\mathcal{G}_c$, respectively. If for all pairs of graph signals $\boldsymbol{x}, \boldsymbol{y} \in \mathbb{R}^n$, the inner product between the two signals is preserved under the coarsening process, i.e.:*

$$\boldsymbol{x}^\top \boldsymbol{L}\boldsymbol{y} = \boldsymbol{x}_c^\top \boldsymbol{L}_c \boldsymbol{y}_c,$$

then the graph Laplacian of the original graph, $\boldsymbol{L}$, can be fully reconstructed from $\boldsymbol{L}_c$ via:

$$\boldsymbol{L} = \boldsymbol{L}_l = \boldsymbol{P}^\top \boldsymbol{L}_c \boldsymbol{P}$$

See App. A.1 for proof. Prop. 3.2 shows that preserving inner products of graph signals maintains key structural properties, enabling graph reconstruction. We note that a necessary condition for the assumption in Proposition 3.2 to hold is that $\mathrm{rank}(\boldsymbol{L}) < k$, which implies that the graph has at least $n - k$ connected components, a condition that is rarely met in practice. Yet, we show in Sec. 4 that our approach achieves the lowest reconstruction error (RE) among baselines, even when this criterion is violated, demonstrating its broad applicability. In Sec. 3.1, we provide analytical evidence that minimizing IPE leads to the minimization of other coarsening metrics as well.

Preserving inner products using the Grassmann manifold. We propose an optimization approach for graph coarsening to preserve inner products between graph signals. The objective function and constraints are given by:

$$\min_{\boldsymbol{C}} f(\boldsymbol{C}) = \|\boldsymbol{X}^\top \boldsymbol{L}\boldsymbol{X} - \boldsymbol{X}_c^\top \boldsymbol{L}_c \boldsymbol{X}_c\|_F^2 - \beta Gr(\boldsymbol{C}, \boldsymbol{U}^{(k)}) + \lambda g(\boldsymbol{C}) + \alpha h(\boldsymbol{L}_c) \tag{8}$$

$$\text{s.t.} \quad \boldsymbol{L}_c = \boldsymbol{C}^T \boldsymbol{L}\boldsymbol{C}, \boldsymbol{X}_c = \boldsymbol{C}^\dagger \boldsymbol{X}, \boldsymbol{C} \in \mathcal{C}$$

where $\boldsymbol{C} \in \mathbb{R}^{n \times k}$ is the coarsening operator; $\boldsymbol{L} \in \mathbb{R}^{n \times n}$ and $\boldsymbol{X} \in \mathbb{R}^{n \times p}$ are the given graph Laplacian and feature matrix of the original graph; $\boldsymbol{U}^{(k)}$ is a matrix containing the k leading eigenvectors of $\boldsymbol{L}$; $\boldsymbol{L}_c \in \mathbb{R}^{k \times k}$ and $\boldsymbol{X}_c \in \mathbb{R}^{k \times p}$ are the Laplacian and feature matrix of the coarsened graph, and $\mathcal{C}$ is the set defined in (7). The function $Gr(\cdot, \cdot)$ is the Grassmann similarity score defined in (3), and functions $h(\cdot)$ and $g(\cdot)$ are regularization functions for $\boldsymbol{L}_c$ and $\boldsymbol{C}$, while $\lambda, \alpha > 0$ are positive regularization parameters.

The objective in (8) minimize the IPE using two complementary terms. The first involves directly minimizing the IPE on the given node features. Although this improves performance on the available data, it does not generalize well to new signals, as its effectiveness depends heavily on the specific information encoded in the feature matrix $\boldsymbol{X}$. The second term aims to maximize the Grassmann similarity (3) between the coarsening matrix $\boldsymbol{C}$ and the leading eigenvectors $\boldsymbol{U}^{(k)}$ of $\boldsymbol{L}$. In Sec. 3.1, we show analytically that this alignment promotes IPE minimization for general unseen smooth signals, e.g., satisfying a smoothness assumption (Prop. 3.4), and preserves important structural properties (Prop. 3.5). The parameter β balances the two terms, adjusting the emphasis between performance on the observed data and generalization to new signals. Our empirical results show that both terms contribute to the coarsening process.

Proposed algorithms. One limitation of the objective in (8) is that the derivative of the first term does not have a closed-form expression with respect to $\boldsymbol{C}$. As a remedy, we adopt the multi-block optimization framework suggested by Kumar et al. [14], recasting our objective function as:

$$\begin{aligned}\min_{\boldsymbol{C}} f(\boldsymbol{X}_c,\boldsymbol{C}) = \|\boldsymbol{X}^\top \boldsymbol{L}\boldsymbol{X} - \boldsymbol{X}_c^\top \boldsymbol{C}^\top \boldsymbol{L}\boldsymbol{C}\boldsymbol{X}_c\|_F^2 - \beta tr(\boldsymbol{U}^{(k)}(\boldsymbol{U}^{(k)})^\top \boldsymbol{C}\boldsymbol{C}^\top) \\ + \lambda\|\boldsymbol{C}^T\|_{1,2}^2 - \alpha \log\det(\boldsymbol{C}^\top \boldsymbol{L}\boldsymbol{C} + \boldsymbol{J}) \\ \textbf{s.t.} \qquad \boldsymbol{X}_c = \boldsymbol{C}^\dagger \boldsymbol{X}, \quad \boldsymbol{C} \in \mathcal{C}\end{aligned} \tag{9}$$

where the terms involving Grassmann similarity and $\boldsymbol{L}_c$ are written explicitly. We adopt the same regularization functions as in Kumar et al. [14], which promote balanced super-node assignment and connectivity in the coarsened graph. The function $g(\boldsymbol{C}) = \|\boldsymbol{C}^\top\|_{1,2}^2 = \sum_{i=1}^{n}\left(\sum_{j=1}^{k}|C_{i,j}|\right)^2$ is an $l_{1,2}$-based group penalty that, as shown in [24, 14], encourages valid coarsening operators. The second regularization term is $h(\boldsymbol{L}_c) = \log\det(\boldsymbol{L}_c + \boldsymbol{J})$, where $\boldsymbol{J} = \frac{1}{k}\mathbf{1}_{k\times k}$. This term ensures that $\boldsymbol{L}_c + \boldsymbol{J}$ is full rank, implying $\mathrm{rank}(\boldsymbol{L}_c) = k-1$, which guarantees that the coarsened graph $\mathcal{G}_c$ is connected [25, 26].

In this recast, the derivative of the modified objective function has a closed-form expression with respect to $\boldsymbol{C}$, and the gradient is presented in App. A.4. We optimize this objective by applying projected gradient descent [27] to estimate the matrix $\boldsymbol{C}$. Specifically, applying ordinary gradient descent steps could deviate from the feasible set $\mathcal{C}$ on the Grassmann manifold. Therefore, we use projected gradient descent to periodically project $\boldsymbol{C}$ back onto the Grassmann manifold after a fixed number of gradient descent steps using the operator Hardmax($\boldsymbol{C}$). Hardmax($\boldsymbol{C}$) applies a hard maximum at each row of $\boldsymbol{C}$, ensuring column-wise orthogonality, which coincides with the structural constraints of the Grassmann manifold.

A full description of this method is in Algorithm 1, termed INGC. In Algorithm 2 , we present another version, where we omit the first term in (9). In this case, we denote the algorithm's objective function by $\tilde{f}(\boldsymbol{C})$. This version focuses on minimizing the IPE via Grassmann similarity, removes dependence on the feature matrix $\boldsymbol{X}$, and enables estimating $\boldsymbol{C}$ using standard gradient descent. We refer to this algorithm as We note that, for SINGC, we empirically observed that projecting only once at the end of the optimization yields performance similar to using intermediate projections, as done for INGC. Therefore, for simplicity and efficiency, we chose to apply standard gradient descent throughout the iterations and perform the projection using Hardmax($\boldsymbol{C}$) only at the end.

Algorithm 1 INGC Algorithm

Input: $\boldsymbol{L} \in \mathbb{R}^{n\times n}, \boldsymbol{X} \in \mathbb{R}^{n\times p}$
Parameters: $\beta, \lambda, \alpha, \eta, t_{iter}, c_{iter}$
Output: $\boldsymbol{L}_c \in \mathbb{R}^{k\times k}, \boldsymbol{X}_c \in \mathbb{R}^{k\times p}$

Compute $\boldsymbol{U}^{(k)}$.
Initialize $\boldsymbol{C}_0$, $t = 0$.
while $\|\boldsymbol{C}_{t+1} - \boldsymbol{C}_t\|_F < \epsilon_C$ or $t < t_{iter}$ **do**
  $\boldsymbol{C}_{t(0)} = \boldsymbol{C}_t$.
  Compute $\nabla_{\boldsymbol{C}} f(\boldsymbol{X}_c, \boldsymbol{C})$ (see (16))
  for i in range(c_{iter}) **do**
    Update $\boldsymbol{C}_{t+1}$ using the gradient descent step:
    $\boldsymbol{C}_{t(i+1)} \leftarrow \boldsymbol{C}_{t(i)} - \eta\nabla_{\boldsymbol{C}} f(\boldsymbol{X}_{c(t)}, \boldsymbol{C}_{t(i)})$
  end for
  $\boldsymbol{C}_{t+1} = \text{Hardmax}(\boldsymbol{C}_{t(c_{iter})})$
  $\boldsymbol{X}_{c(t+1)} = \boldsymbol{C}_{t+1}^\dagger X, \quad t = t+1$
end while
Hardmax(C)
return $\boldsymbol{L}_c = \boldsymbol{C}_t^\top \boldsymbol{L}\boldsymbol{C}, \boldsymbol{X}_c = \boldsymbol{C}_t^\dagger \boldsymbol{X}$

Algorithm 2 SINGC Algorithm

Input: $\boldsymbol{L} \in \mathbb{R}^{n\times n}$
Parameters: $\lambda, \alpha, \eta, t_{iter}$
Output: $\boldsymbol{L}_c \in \mathbb{R}^{k\times k}$

Compute $\boldsymbol{U}^{(k)}$.
Initialize $\boldsymbol{C}_0$, $t = 0$.
while $\|\boldsymbol{C}_{t+1} - \boldsymbol{C}_t\|_F < \epsilon_C$ or $t < t_{iter}$ **do**
  Compute $\nabla_{\boldsymbol{C}} \tilde{f}(\boldsymbol{C})$ (see (17))
  Update $\boldsymbol{C}_{t+1}$ using the gradient descent step:
  $\boldsymbol{C}_{t+1} \leftarrow \boldsymbol{C}_t - \eta\nabla_{\boldsymbol{C}} \tilde{f}(\boldsymbol{C}_t)$
  $t = t+1$
end while
Hardmax(C)
return $\boldsymbol{L}_c = \boldsymbol{C}_t^\top \boldsymbol{L}\boldsymbol{C}$

3.1 Theoretical analysis

Next, we present two key analytical results. First, we show that the second term in (8) minimizes the IPE for general smooth graph signals. Second, we connect this minimization and common graph coarsening metrics, such as DEE and REE. We begin by defining a smooth graph signal. Dong et al. [28] model a smooth graph signal generation mechanism as:

$$\boldsymbol{x} = \boldsymbol{U}\boldsymbol{h} + \epsilon_\eta \boldsymbol{\eta}, \tag{10}$$

where $\boldsymbol{L} = \boldsymbol{U}\boldsymbol{\Lambda}\boldsymbol{U}^\top$ is the Laplacian of the respective graph signal, $\boldsymbol{h} \sim \mathcal{N}(0, \boldsymbol{\Lambda}^\dagger) \in \mathbb{R}^n$, $\boldsymbol{\eta} \sim \mathcal{N}(0, \boldsymbol{I}_{n\times n}) \in \mathbb{R}^n$, and $\epsilon_\eta > 0$ is the noise standard deviation. This model suggests that a smooth graph signal is a combination of the first eigenvectors of $\boldsymbol{L}$ and scaled noise.

Assumption 3.3 (k-smooth graph signal [29]) *A graph signal $\boldsymbol{x} \in \mathbb{R}^n$ is termed "k-smooth" on the graph $\mathcal{G}$ if it can be fully expressed by the first k eigenvectors of its corresponding Laplacian $\boldsymbol{L}$, i.e., $\boldsymbol{x} = \sum_{i=1}^k c_i \boldsymbol{u}^{(i)} = \boldsymbol{c}(\boldsymbol{U}^{(k)})^\top$ where the columns of $\boldsymbol{U}^{(k)} = [\boldsymbol{u}^{(1)}, \ldots, \boldsymbol{u}^{(k)}] \in \mathbb{R}^{n\times k}$ are the k-leading eigenvectors of $\boldsymbol{L}$.*

Table 4 in App. E shows the extent to which this assumption holds in real datasets. Based on Assumption 3.3, the following result provides motivation to incorporate the Grassmann similarity score $Gr(\boldsymbol{C}, \boldsymbol{U}^{(k)})$ defined in (3) into our proposed objective.

Proposition 3.4 *Let $\boldsymbol{X}$ be a feature matrix of a graph $\mathcal{G}$ with a Laplacian matrix $\boldsymbol{L}$, where each column of $\boldsymbol{X}$ is k-smooth on the graph $\mathcal{G}$. Then, any mapping $\boldsymbol{L}_c = \boldsymbol{C}\boldsymbol{L}\boldsymbol{C}^\top, \boldsymbol{X}_c = \boldsymbol{C}^\top\boldsymbol{X}$, such that $\boldsymbol{C} = \boldsymbol{U}^{(k)}\boldsymbol{O}$ satisfies:*

$$\|\boldsymbol{X}^\top\boldsymbol{L}\boldsymbol{X} - \boldsymbol{X}_c^\top\boldsymbol{L}_c\boldsymbol{X}_c\|_F^2 = 0$$

where the columns of $\boldsymbol{U}^{(k)} \in \mathbb{R}^{n\times k}$ are the k-leading eigenvectors of $\boldsymbol{L}$, and $\boldsymbol{O} \in \mathcal{SO}(k)$.

See App. A.2 for proof. Proposition 3.4 implies that any coarsening operator $\boldsymbol{C}$ whose columns span the same subspace as $\boldsymbol{U}^{(k)}$ minimizes the IPE in (3.1) for any k-smooth signals on the original graph. Thus, the second term in our objective (8) maximizes the Grassmann similarity (3) between $\boldsymbol{C}$ and $\boldsymbol{U}^{(k)}$, aiming to find a valid coarsening operator (i.e., $\boldsymbol{C} \in \mathcal{C}$) that satisfies $\boldsymbol{C} = \boldsymbol{U}^{(k)}\boldsymbol{O}$.

Next, we present a theorem that provides bounds on the DEE (Def. 2.4) and REE (Def. 2.1) as functions of ϵ, which quantifies the deviation of the second term in our objective from its optimal value (if $\boldsymbol{C}$ and $\boldsymbol{U}^{(k)}$ span the same subspace, then $\text{tr}(\boldsymbol{U}^{(k)}(\boldsymbol{U}^{(k)})^\top\boldsymbol{C}\boldsymbol{C}^\top) = k$).

Proposition 3.5 *Let $\boldsymbol{L}$ be the Laplacian of a connected graph $\mathcal{G}$, and let $\boldsymbol{U}^{(k)}$ be the matrix containing its k-leading eigenvectors. Suppose $\boldsymbol{L}_c = \boldsymbol{C}^\top\boldsymbol{L}\boldsymbol{C}$ is the Laplacian of a coarsened graph derived using a coarsening operator $\boldsymbol{C}$ such that $tr(\boldsymbol{U}^{(k)}(\boldsymbol{U}^{(k)})^\top\boldsymbol{C}\boldsymbol{C}^\top) = k - \epsilon$, and the constant vector in $\mathbb{R}^n$ is spanned by the columns of $\boldsymbol{C}$. Then, the eigenvalues of the original graphs $\{\lambda^i\}_{i=1}^k$ and the coarsened graph $\{\lambda_c^i\}_{i=1}^k$ satisfy,*

$$\frac{1}{\mu_1}\lambda^{(i)} \leq \lambda_c^{(i)} \leq \frac{1}{\mu_k}\frac{(1+\epsilon\kappa)^2}{1-(\epsilon\kappa)^2(\lambda^{(i)}/\lambda^{(2)})}\lambda^{(i)}, \quad 2 \leq i \leq k$$

and the Dirichlet energies of a k-smooth graph signal $\boldsymbol{x}$ on the graph, the inequalities:

$$(1-\epsilon\kappa)^2\|\boldsymbol{x}\|_L \leq \|\boldsymbol{x}_c\|_{L_c} \leq (1+\epsilon\kappa)^2\|\boldsymbol{x}\|_L,$$

whenever $\epsilon\kappa < \frac{\lambda^{(2)}}{\lambda^{(i)}}$. Here $\kappa = \frac{\lambda_{max}(\boldsymbol{L})}{\lambda^{(2)}}$, $\lambda_{max}(\boldsymbol{L})$ is the maximum eigenvalue of $\boldsymbol{L}$,$\boldsymbol{P} = \boldsymbol{C}^\dagger$, μ_1,μ_k and the first and k eigenvalues of the matrix $\boldsymbol{P}\boldsymbol{P}^\top$, $\|\boldsymbol{x}\|_L = \boldsymbol{x}^T\boldsymbol{L}\boldsymbol{x}$, $\|\boldsymbol{x}_c\|_{L_c} = \boldsymbol{x}_c^T\boldsymbol{L}_c\boldsymbol{x}_c$.

See App.A.3 for proof. Prop. 3.5 shows that the bounds for both REE (Def. 2.1) and DEE (Def. 2.4) become tighter as ϵ decreases. Combining Prop. 3.4 and 3.5 implies that minimizing the IPE for general smooth signals reduces both the REE and DEE graph coarsening metrics.

Complexity. Our approach formulates coarsening as an optimization problem, so its applicability depends on both computational complexity and convergence time. In App. C, we compare the complexity of our methods with FGC [14], an optimization-based coarsening approach considered

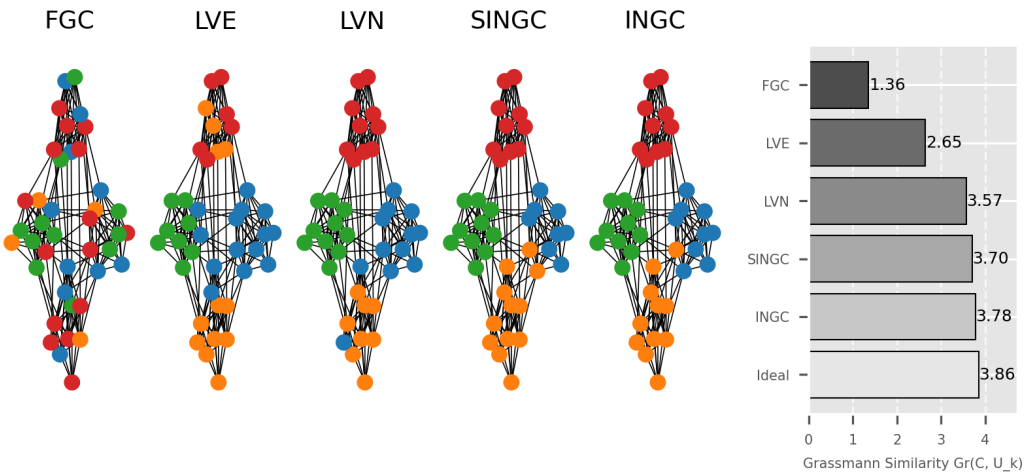

Figure 1: Node assignments of all methods on a synthetic graph generated from an SBM. Nodes with the same color belong to the same class (super-node). The bar plot on the right shows the Grassmann similarity between each method's coarsening matrix $\boldsymbol{C}$ and the leading four eigenvectors $\boldsymbol{U}^{(k)}$ of the graph Laplacian. The bottom bar shows the similarity for the ideal partitioning—i.e., between the block-model-based $\boldsymbol{C}$ and $\boldsymbol{U}^{(k)}$. The maximum similarity in this case is 4.

state-of-the-art on many benchmarks, which has been shown to accelerate GNNs training time. We show that our methods are similarly efficient while achieving better results. Moreover, we show that applying coarsening before a GCN is particularly advantageous for dense graphs with significantly more edges than nodes. Runtime comparisons supporting this claim are presented in App. C. Finally, App. D provides convergence plots illustrating the trade-off between speed and final objective value.

4 Experimental results

Visual illustration. A key aspect of graph coarsening is how well the global graph's structure is preserved. This can be assessed by how effectively the partitioning into super-nodes captures it. To illustrate this property, we provide a visual example showing how the super-nodes generated by our method align with the graph's global structure. This example highlights how our approach maintains a meaningful graph representation, despite focusing solely on functional relationships.

The example is based on a synthetic graph generated using a Stochastic Block Model (SBM) [30] with four classes, each containing 10 vertices ($N = 40$), an intra-class probability of $p = 0.9$, and an inter-class probability of $q = 0.05$. The feature matrix $\boldsymbol{X}$ is generated following the same graph signal generation mechanism described in (10). We set the target coarsened graph for all coarsening methods to have $k = 4$ super-nodes. In Figure 1, we present the results obtained by our methods (INGC/SINGC), alongside three other graph coarsening baselines: Feature-based Graph Coarsening (FGC) [14], which incorporates node features into the coarsening process, and the Local Variation Neighborhood (LVN) and Local Variation Edges (LVE) methods [10], which use the original graph Laplacian eigenvectors as part of their coarsening objectives. We observe that the super-nodes assignment of our methods closely aligns with the partitioning of the nodes to four classes according to the SBM, as indicated by the node colors in Figure 1. On the right-hand side of Figure 1, we present a bar plot comparing the Grassmann similarity between the coarsening matrices $\boldsymbol{C}$ (which encode the vertex partitioning) produced by each method and the top four eigenvectors of the original graph Laplacian, $\boldsymbol{U}^{(k)}$. The bottom bar represents the matrix $\boldsymbol{C}$ that encodes the ideal partition based on the underlying block model of the graph, serving as a baseline. We observe that our method achieves the highest similarity, closely approaching the ideal partitioning. Note that when the coarsening matrix $\boldsymbol{C}$ and the eigenvector matrix $\boldsymbol{U}^{(k)}$ span the same subspace, the Grassmann similarity reaches its maximum of 4. This comparison highlights our motivation for incorporating Grassmann similarity into our coarsening objective, as it preserves the graph's global structure. Numerically, this property is reflected in the REE metric; we present an extensive evaluation of this and other metrics in the following section. For more visual comparisons, see App.B.

Table 1: Comparison of coarsening methods on four datasets using multiple metrics and coarsening ratios (r). For each method, we report REE, RE, HE, DEE, and INP on each dataset. Best results are in bold; second-best are underlined. The last two columns count how often each method achieved the best or second-best performance.

Method		Karate Club			Les Miserables			Cora			Citeseer			#Best	#2-Best
	r	0.7	0.5	0.3	0.7	0.5	0.3	0.7	0.5	0.3	0.7	0.5	0.3		
LVN	REE	**0.30**	1.52	3.15	0.36	1.39	7.82	**0.57**	1.31	4.23	**0.68**	1.58	4.11	3	4
	RE	9.71	9.87	10.31	11.42	11.91	11.91	11.42	11.62	11.70	10.85	11.05	11.14	0	0
	HE	1.74	1.89	2.25	1.92	2.60	2.54	1.89	2.50	3.17	1.93	2.52	3.43	0	0
	DEE	36.2	47.8	46.6	65.1	99.4	90.2	39.1	70.7	90.2	40.0	66.3	111.1	0	0
	IPE	0.71	0.72	1.09	2.02	2.56	1.91	2.87	2.23	1.73	0.93	0.98	1.09	0	0
LVE	REE	0.82	**0.48**	**2.26**	1.05	4.56	**7.60**	0.81	1.94	5.14	0.79	1.62	4.26	3	2
	RE	9.39	9.91	9.97	11.55	12.14	12.48	10.62	11.51	11.69	10.52	11.02	11.14	0	0
	HE	1.40	1.93	2.31	1.63	2.16	2.89	1.29	2.31	3.10	1.61	2.50	3.40	0	0
	DEE	17.3	39.0	84.8	19.1	20.6	63.6	22.5	44.9	78.1	30.1	63.5	109.0	0	0
	IPE	0.66	0.88	0.92	1.59	2.77	3.87	0.58	1.19	1.54	0.61	0.79	0.88	0	0
FGC	REE	1.35	3.94	7.54	3.08	10.31	33.18	1.78	5.40	15.99	1.58	8.92	35.88	0	0
	RE	8.70	8.81	9.26	9.97	9.98	10.91	9.70	10.82	10.76	10.47	10.23	10.31	0	1
	HE	1.03	1.23	1.80	0.82	0.87	1.58	0.76	1.40	1.56	1.89	1.39	1.61	0	2
	DEE	8.05	11.57	21.36	4.78	7.65	9.74	0.20	0.41	5.01	19.5	7.87	1.34	0	1
	IPE	0.55	0.58	0.94	1.05	2.17	3.67	0.41	1.01	3.67	1.10	0.49	0.68	0	0
INGC (Ours)	REE	0.78	1.30	2.97	**0.08**	**1.30**	10.40	0.86	**0.84**	**0.76**	0.71	**0.62**	**0.42**	6	4
	RE	6.27	**7.00**	**8.28**	**5.43**	**8.08**	**9.79**	**9.49**	**10.17**	**10.42**	**8.86**	9.85	10.10	9	3
	HE	0.29	**0.45**	**1.00**	**0.08**	**0.33**	**0.83**	**0.67**	**1.04**	**1.37**	**0.64**	1.21	1.61	9	3
	DEE	**0.01**	**0.03**	**0.02**	**0.04**	**0.02**	**0.10**	**0.03**	**0.40**	**3.12**	**0.02**	**0.66**	1.01	11	1
	IPE	0.19	**0.31**	**0.48**	0.30	**0.57**	**0.86**	**0.31**	**0.43**	**0.68**	**0.24**	0.34	0.58	8	4
SINGC (Ours)	REE	0.86	1.78	4.02	0.50	2.32	7.78	0.86	**0.84**	5.10	0.83	**0.62**	**0.42**	3	0
	RE	**6.09**	8.05	8.74	9.07	9.60	10.49	9.54	**10.17**	10.95	9.32	**9.76**	**9.92**	4	7
	HE	**0.27**	0.85	1.46	0.51	0.72	1.29	0.69	**1.04**	1.84	0.83	**1.14**	**1.27**	4	7
	DEE	0.02	0.51	6.56	0.47	0.35	**0.10**	**0.03**	**0.40**	8.12	1.01	1.45	**0.10**	4	7
	IPE	**0.19**	0.43	0.59	**0.21**	0.63	1.07	**0.31**	**0.43**	0.69	0.27	**0.25**	**0.47**	6	6

Graph coarsening metrics. Here, we evaluate the performance of our methods on several benchmark datasets using the coarsening metrics from Sec. 2. We compare them with current SOTA coarsening methods—LVN and LVE—which are known to perform best on structural-preservation metrics (e.g., REE, RE), and FGC, which is considered the leading method for metrics that also consider the features of the nodes. We conduct experiments on four datasets: The Karate Club[31], Les Miserables[32], Cora[33], and Citeseer[34]. Note that the Cora and Citeseer datasets include node features, whereas the Karate Club and Les Miserables datasets do not. For the latter two, we generated node features using the signal generation mechanism presented in Section 3.1.

Table 1 summarizes the performance of our methods (INGC and SINGC) and the baselines (FGC, LVN and LVE) across different datasets and coarsening ratios ($r = \frac{k}{n} = 0.7$, 0.5, and 0.3). The best performance for each metric is highlighted in bold, and the second-best is underlined. The last two columns summarize the number of settings in which each method achieved the lowest or second-lowest score compared to others. We observe that INGC achieves the best overall performance across all graph metrics. SINGC, a more efficient variant, is also highly competitive—often ranking second and occasionally achieving the best results. Baseline methods (LVN, LVE, and FGC) show mixed performance. LVN and LVE perform well on REE for some datasets, indicating good spectral preservation, but generally underperform on metrics involving node features. FGC, the only baseline that incorporates node features in coarsening, outperforms the others on related metrics. However, both our methods consistently surpass FGC. The strong RE score of our approach demonstrates its broader ability to preserve graph structure, even beyond the theoretical setting of Theorem 3.2, as the datasets used are connected or have far fewer than $n - k$ connected components.

The hyperparameters in these experiments were selected via grid search, a standard approach in graph coarsening when aiming to minimize a specific metric. The best results for each metric were obtained using different hyperparameters, as reported in App. G.3. This variability highlights the

Table 2: Node classification accuracy across datasets and coarsening ratios (r). Best results are bolded; second-best are underlined. The last two rows count best and second-best results per method.

Dataset	r	GCOND	SCAL(LV)	FGC	MGC	INGC (Ours)	SINGC (Ours)
Cora	0.3	81.56 ± 0.60	79.42 ± 1.71	$\underline{85.79 \pm 0.24}$	84.56 ± 1.40	$\mathbf{87.55 \pm 0.16}$	84.51 ± 0.33
	0.1	81.37 ± 0.40	71.38 ± 3.62	81.46 ± 0.79	76.02 ± 0.93	$\mathbf{83.38 \pm 0.47}$	$\underline{82.76 \pm 0.32}$
	0.05	$\underline{79.93 \pm 0.44}$	55.32 ± 7.03	$\mathbf{80.01 \pm 0.51}$	-	77.42 ± 0.78	77.81 ± 0.68
Citeseer	0.3	72.43 ± 0.94	68.87 ± 1.37	74.64 ± 1.37	74.60 ± 1.20	$\mathbf{76.89 \pm 0.23}$	$\underline{76.66 \pm 0.27}$
	0.1	70.46 ± 0.47	71.38 ± 3.62	$\mathbf{73.36 \pm 0.53}$	70.57 ± 1.25	$\underline{72.63 \pm 0.25}$	69.71 ± 0.72
	0.05	64.03 ± 2.40	55.32 ± 7.03	$\mathbf{71.02 \pm 0.96}$	-	66.02 ± 0.32	$\underline{66.37 \pm 0.57}$
Co-phy	0.05	93.05 ± 0.26	73.09 ± 7.41	94.27 ± 0.25	$\mathbf{94.52 \pm 0.19}$	$\underline{94.29 \pm 0.10}$	94.04 ± 0.06
	0.03	92.81 ± 0.31	63.65 ± 9.65	$\underline{94.02 \pm 0.20}$	$\underline{93.64 \pm 0.25}$	$\mathbf{94.20 \pm 0.13}$	93.52 ± 0.13
	0.01	92.79 ± 0.40	31.08 ± 2.65	93.08 ± 0.22	-	$\mathbf{93.95 \pm 0.20}$	$\underline{93.20 \pm 0.10}$
Pubmed	0.05	78.16 ± 0.30	72.82 ± 2.62	80.73 ± 0.44	81.89 ± 0.01	$\mathbf{83.59 \pm 0.22}$	$\underline{83.55 \pm 0.32}$
	0.03	78.04 ± 0.47	70.24 ± 2.63	79.91 ± 0.30	80.70 ± 0.01	$\underline{81.93 \pm 0.22}$	$\mathbf{83.19 \pm 0.18}$
	0.01	77.20 ± 0.20	54.49 ± 10.5	78.42 ± 0.43	-	$\underline{79.09 \pm 0.26}$	$\mathbf{79.96 \pm 0.34}$
Co-CS	0.05	86.29 ± 0.63	34.45 ± 10.0	89.60 ± 0.39	-	$\underline{90.84 \pm 0.12}$	$\mathbf{90.92 \pm 0.22}$
	0.03	86.32 ± 0.45	26.06 ± 9.29	88.29 ± 0.79	-	$\underline{89.59 \pm 0.38}$	$\mathbf{89.99 \pm 0.41}$
	0.01	84.01 ± 0.02	14.42 ± 8.50	$\underline{86.37 \pm 1.36}$	-	$\mathbf{87.93 \pm 0.33}$	83.39 ± 0.33
#Best		0	0	3	1	7	4
#2-Best		1	0	3	1	5	4

need to tune hyperparameters based on the specific application and the most relevant coarsening metric. For example, minimizing REE may be crucial for clustering, while tasks like graph pooling and node classification—which rely heavily on node features—benefit from prioritizing DEE and INP during tuning. App. F presents a hyperparameter study showing each parameter's contribution and sensitivity across metrics.

Node classification. Next, we evaluate our method on node classification using several benchmark datasets. This task assesses how well coarsened graphs preserve structural and feature information for accurate label prediction [4]. Following Kumar et al. [14], we train a Graph Neural Network (GNN) on the coarsened graph and predict node labels for the original graph, reducing training time due to fewer nodes and edges. Specifically, we: (1) generate a coarsened graph using a selected method; (2) compute super-node labels via $\boldsymbol{y}_c = \boldsymbol{C}^\dagger \boldsymbol{y}$; (3) train a GNN on the coarsened graph; and (4) evaluate predictions $\hat{\boldsymbol{y}} = \text{GNN}(\boldsymbol{L}, \boldsymbol{X})$ against the original labels $\boldsymbol{y}$. Note that this task is used solely for evaluation, with all labels $\boldsymbol{y}$ available throughout.

We replicated the experimental settings from Kumar et al. [14] and Huang et al. [35], both of which employ a Graph Convolutional Network (GCN) [36]. We then compared the performance of our methods (INGC and SINGC) with the top-performing methods in those papers that are considered to be SOTA, namely SCAL [35], Featured Graph Coarsening (FGC) [14], Graph Condensation (GCOND) [7], and Multi-Component Coarsening (MGC) [37]. The datasets include two medium-sized graphs (Cora and Citeseer) and three large-scale graphs (Co-Physics, Pubmed, and Co-CS). Each method's effectiveness was evaluated using 10-fold cross-validation. A detailed description of the experimental setup is in App. G.2.

The results are reported in Table 2 with mean accuracy and standard deviation across the folds for each method at different coarsening ratios r. We observe that INGC outperforms the SOTA methods on large datasets (Co-Physics, Pubmed, and Co-CS), and matches their performance on medium-sized datasets. SINGC outperforms baseline methods in most settings, despite having a simpler optimization objective. A key takeaway from the results is that the integration of node features into the coarsening process gives FGC, INGC and SINGC a competitive advantage over methods that primarily focus on structural properties, such as SCAL and GCOND, as was also indicated in [14]. This relationship is intuitive, as node classification relies not only on structural relationships but also on the meaningful preservation of node features.

App. F presents an ablation study on β, highlighting the role of the Grassmann similarity term. App. E discusses Assumption 3.3, evaluates its validity on real datasets, and shows our method remains effective even when it is not fully met. Moreover, our empirical results indicate that SINGC benefits when a larger fraction of signal energy resides in the low-frequency band, and its best performance reported on PubMed, where this assumption is most valid.

The source code for all experiments is available at: `Code`.

5 Conclusion

In this paper, we introduced a new graph coarsening method that focuses on preserving the inner products of graph signals during the coarsening process. We demonstrated that, although primarily considering node features, our approach also maintains the global structure of the graph. Our methods, INGC and SINGC, outperform state-of-the-art techniques across various graph coarsening metrics and tasks (e.g., node classification), showcasing their versatility and effectiveness in preserving essential graph properties. These results highlight the potential of our approach for graph-based learning applications. However, similar to other optimization-based coarsening techniques, our method faces scalability limitations when applied to extremely large graphs. This challenge may be addressed in practical scenarios by partitioning the graph into manageable subgraphs, processing each subgraph independently, potentially in parallel, and subsequently reconnecting them [38]. A critical assumption underlying our work is that the node features exhibit smoothness with respect to the graph topology, an attribute closely related to homophily. Consequently, our evaluation is restricted to homophilic graphs. For future research, an extension to heterophilic datasets could involve adapting the second term in our objective to facilitate alignment with alternative frequency bands. For example, the low-frequency basis $\boldsymbol{U}^{(k)}$ may be replaced with a different basis representing mid or high frequencies, guided by prior knowledge of label–frequency alignment. Future directions also include integrating our coarsening into graph pooling and evaluating its impact on improving GNN performance.

Acknowledgments

We thank the anonymous reviewers for their insightful feedback. This work was supported by the European Union's Horizon 2020 research and innovation programme under grant agreement No. 802735-ERC-DIFFOP.

References

[1] Stanley Wasserman and Katherine Faust. Social network analysis: Methods and applications. 1994.

[2] Georgios A Pavlopoulos, Maria Secrier, Charalampos N Moschopoulos, Theodoros G Soldatos, Sophia Kossida, Jan Aerts, Reinhard Schneider, and Pantelis G Bagos. Using graph theory to analyze biological networks. *BioData mining*, 4:1–27, 2011.

[3] Maarten Van Steen. Graph theory and complex networks. *An introduction*, 144(1), 2010.

[4] Mohammad Hashemi, Shengbo Gong, Juntong Ni, Wenqi Fan, B Aditya Prakash, and Wei Jin. A comprehensive survey on graph reduction: Sparsification, coarsening, and condensation. *arXiv preprint arXiv:2402.03358*, 2024.

[5] Joshua D Batson, Daniel A Spielman, and Nikhil Srivastava. Twice-ramanujan sparsifiers. In *Proceedings of the forty-first annual ACM symposium on Theory of computing*, pages 255–262, 2009.

[6] Ryan Wickman, Xiaofei Zhang, and Weizi Li. A generic graph sparsification framework using deep reinforcement learning. In *2022 IEEE International Conference on Data Mining (ICDM)*, pages 1221–1226. IEEE, 2022.

[7] Wei Jin, Lingxiao Zhao, Shichang Zhang, Yozen Liu, Jiliang Tang, and Neil Shah. Graph condensation for graph neural networks. *arXiv preprint arXiv:2110.07580*, 2021.

[8] Yang Liu, Deyu Bo, and Chuan Shi. Graph condensation via eigenbasis matching. *arXiv preprint arXiv:2310.09202*, 2023.

[9] Jie Chen, Yousef Saad, and Zechen Zhang. Graph coarsening: from scientific computing to machine learning. *SeMA Journal*, 79(1):187–223, 2022.

[10] Andreas Loukas and Pierre Vandergheynst. Spectrally approximating large graphs with smaller graphs. In *International conference on machine learning*, pages 3237–3246. PMLR, 2018.

[11] Kristen LeFevre and Evimaria Terzi. Grass: Graph structure summarization. In *Proceedings of the 2010 SIAM International Conference on Data Mining*, pages 454–465. SIAM, 2010.

[12] Yuanyuan Tian, Richard A Hankins, and Jignesh M Patel. Efficient aggregation for graph summarization. In *Proceedings of the 2008 ACM SIGMOD international conference on Management of data*, pages 567–580, 2008.

[13] Sorour E Amiri, Bijaya Adhikari, Aditya Bharadwaj, and B Aditya Prakash. Netgist: Learning to generate task-based network summaries. In *2018 IEEE International Conference on Data Mining (ICDM)*, pages 857–862. IEEE, 2018.

[14] Manoj Kumar, Anurag Sharma, Shashwat Saxena, and Sandeep Kumar. Featured graph coarsening with similarity guarantees. In *International Conference on Machine Learning*, pages 17953–17975. PMLR, 2023.

[15] Ioan Mackenzie James. *The topology of Stiefel manifolds*, volume 24. Cambridge University Press, 1976.

[16] Thomas Bendokat, Ralf Zimmermann, and P-A Absil. A grassmann manifold handbook: Basic geometry and computational aspects. *arXiv preprint arXiv:2011.13699*, 2020.

[17] Alan Edelman, Tomás A Arias, and Steven T Smith. The geometry of algorithms with orthogonality constraints. *SIAM journal on Matrix Analysis and Applications*, 20(2):303–353, 1998.

[18] Ido Cohen and Ronen Talmon. Functorial comparison of graph signals using the geodesic distance on the grassmann manifold. *arXiv preprint arXiv:2406.06989*, 2024.

[19] Ulrike Von Luxburg. A tutorial on spectral clustering. *Statistics and computing*, 17:395–416, 2007.

[20] Andreas Loukas. Graph reduction with spectral and cut guarantees. *Journal of Machine Learning Research*, 20(116):1–42, 2019.

[21] Yike Liu, Tara Safavi, Abhilash Dighe, and Danai Koutra. Graph summarization methods and applications: A survey. *ACM computing surveys (CSUR)*, 51(3):1–34, 2018.

[22] Gecia Bravo Hermsdorff and Lee Gunderson. A unifying framework for spectrum-preserving graph sparsification and coarsening. *Advances in Neural Information Processing Systems*, 32, 2019.

[23] Vassilis Kalofolias and Nathanaël Perraudin. Large scale graph learning from smooth signals. *arXiv preprint arXiv:1710.05654*, 2017.

[24] Di Ming, Chris Ding, and Feiping Nie. A probabilistic derivation of lasso and l12-norm feature selections. In *Proceedings of the AAAI conference on artificial intelligence*, volume 33, pages 4586–4593, 2019.

[25] Fan RK Chung. *Spectral graph theory*, volume 92. American Mathematical Soc., 1997.

[26] Vassilis Kalofolias. How to learn a graph from smooth signals. In *Artificial intelligence and statistics*, pages 920–929. PMLR, 2016.

[27] Dimitri P Bertsekas. Nonlinear programming. *Journal of the Operational Research Society*, 48 (3):334–334, 1997.

[28] Xiaowen Dong, Dorina Thanou, Pascal Frossard, and Pierre Vandergheynst. Learning laplacian matrix in smooth graph signal representations. *IEEE Transactions on Signal Processing*, 64 (23):6160–6173, 2016.

[29] Felix Dietrich, Or Yair, Rotem Mulayoff, Ronen Talmon, and Ioannis G Kevrekidis. Spectral discovery of jointly smooth features for multimodal data. *SIAM Journal on Mathematics of Data Science*, 4(1):410–430, 2022.

[30] Emmanuel Abbe. Community detection and stochastic block models: recent developments. *The Journal of Machine Learning Research*, 18(1):6446–6531, 2017.

[31] Wayne W Zachary. An information flow model for conflict and fission in small groups. *Journal of anthropological research*, 33(4):452–473, 1977.

[32] Donald Ervin Knuth. *The Stanford GraphBase: a platform for combinatorial computing*, volume 1. AcM Press New York, 1993.

[33] Andrew Kachites McCallum, Kamal Nigam, Jason Rennie, and Kristie Seymore. Automating the construction of internet portals with machine learning. *Information Retrieval*, 3:127–163, 2000.

[34] C Lee Giles, Kurt D Bollacker, and Steve Lawrence. Citeseer: An automatic citation indexing system. In *Proceedings of the third ACM conference on Digital libraries*, pages 89–98, 1998.

[35] Zengfeng Huang, Shengzhong Zhang, Chong Xi, Tang Liu, and Min Zhou. Scaling up graph neural networks via graph coarsening. In *Proceedings of the 27th ACM SIGKDD conference on knowledge discovery & data mining*, pages 675–684, 2021.

[36] Thomas N Kipf and Max Welling. Semi-supervised classification with graph convolutional networks. *arXiv preprint arXiv:1609.02907*, 2016.

[37] Subhanu Halder, Manoj Kumar, and Sandeep Kumar. Multi-component coarsened graph learning for scaling graph machine learning. In *Companion Proceedings of the ACM on Web Conference 2025*, pages 1001–1004, 2025.

[38] George Karypis and Vipin Kumar. A fast and high quality multilevel scheme for partitioning irregular graphs. *SIAM Journal on scientific Computing*, 20(1):359–392, 1998.

[39] Daniel Spielman. Spectral and algebraic graph theory. *Yale lecture notes, draft of December*, 4: 47, 2019.

[40] Anil K Jain and Richard C Dubes. *Algorithms for clustering data*. Prentice-Hall, Inc., 1988.

[41] Rotem Mulayoff, Tomer Michaeli, and Daniel Soudry. The implicit bias of minima stability: A view from function space. *Advances in Neural Information Processing Systems*, 34:17749–17761, 2021.

[42] Antonio Ortega, Pascal Frossard, Jelena Kovačević, José MF Moura, and Pierre Vandergheynst. Graph signal processing: Overview, challenges, and applications. *Proceedings of the IEEE*, 106 (5):808–828, 2018.

NeurIPS Paper Checklist

1. **Claims**

   Question: Do the main claims made in the abstract and introduction accurately reflect the paper's contributions and scope?

   Answer: [Yes]

   Justification: The abstract and introduction accurately summarize our main contributions: a graph coarsening method that preserves inner products of node features, maintaining both structural and feature fidelity. In Section 3.1, we support our analytical claims, explicitly stating that they hold for signals satisfying a smoothness assumption, as noted in the abstract. The practical advantages of our approach are demonstrated empirically in Section 4.

   Guidelines:

   - The answer NA means that the abstract and introduction do not include the claims made in the paper.
   - The abstract and/or introduction should clearly state the claims made, including the contributions made in the paper and important assumptions and limitations. A No or NA answer to this question will not be perceived well by the reviewers.
   - The claims made should match theoretical and experimental results, and reflect how much the results can be expected to generalize to other settings.
   - It is fine to include aspirational goals as motivation as long as it is clear that these goals are not attained by the paper.

2. **Limitations**

   Question: Does the paper discuss the limitations of the work performed by the authors?

   Answer: [Yes]

   Justification: We address the limitation of formulating coarsening as an optimization problem, including a discussion of its runtime and convergence trade-offs, and the conditions under which it is beneficial (Sec. 3.1 and App.C, D). We also conduct a hyperparameter study (Sec. 4 and App.F) to highlight sensitivity and tuning importance. Additionally, we evaluate the practical validity of our main smoothness assumption across datasets (App. E) and discuss the implications when it is only partially satisfied.

   Guidelines:

   - The answer NA means that the paper has no limitation while the answer No means that the paper has limitations, but those are not discussed in the paper.
   - The authors are encouraged to create a separate "Limitations" section in their paper.
   - The paper should point out any strong assumptions and how robust the results are to violations of these assumptions (e.g., independence assumptions, noiseless settings, model well-specification, asymptotic approximations only holding locally). The authors should reflect on how these assumptions might be violated in practice and what the implications would be.
   - The authors should reflect on the scope of the claims made, e.g., if the approach was only tested on a few datasets or with a few runs. In general, empirical results often depend on implicit assumptions, which should be articulated.
   - The authors should reflect on the factors that influence the performance of the approach. For example, a facial recognition algorithm may perform poorly when image resolution is low or images are taken in low lighting. Or a speech-to-text system might not be used reliably to provide closed captions for online lectures because it fails to handle technical jargon.
   - The authors should discuss the computational efficiency of the proposed algorithms and how they scale with dataset size.
   - If applicable, the authors should discuss possible limitations of their approach to address problems of privacy and fairness.
   - While the authors might fear that complete honesty about limitations might be used by reviewers as grounds for rejection, a worse outcome might be that reviewers discover limitations that aren't acknowledged in the paper. The authors should use their best

judgment and recognize that individual actions in favor of transparency play an important role in developing norms that preserve the integrity of the community. Reviewers will be specifically instructed to not penalize honesty concerning limitations.

3. **Theory assumptions and proofs**

   Question: For each theoretical result, does the paper provide the full set of assumptions and a complete (and correct) proof?

   Answer: [Yes]

   Justification: The paper presents multiple theoretical results, with all assumptions clearly stated in the text and formalized within the propositions. All results that are built on prior work are explicitly referenced. Complete proofs for all propositions are provided in the appendix.

   Guidelines:

   - The answer NA means that the paper does not include theoretical results.
   - All the theorems, formulas, and proofs in the paper should be numbered and cross-referenced.
   - All assumptions should be clearly stated or referenced in the statement of any theorems.
   - The proofs can either appear in the main paper or the supplemental material, but if they appear in the supplemental material, the authors are encouraged to provide a short proof sketch to provide intuition.
   - Inversely, any informal proof provided in the core of the paper should be complemented by formal proofs provided in appendix or supplemental material.
   - Theorems and Lemmas that the proof relies upon should be properly referenced.

4. **Experimental result reproducibility**

   Question: Does the paper fully disclose all the information needed to reproduce the main experimental results of the paper to the extent that it affects the main claims and/or conclusions of the paper (regardless of whether the code and data are provided or not)?

   Answer: [Yes]

   Justification: The paper provides all the necessary details to reproduce the main results. Algorithms 1 and 2 outlines the full optimization procedure, and AppendixG specifies all experimental settings, including dataset descriptions, evaluation metrics, and the exact hyperparameters used for each experiment.

   Guidelines:

   - The answer NA means that the paper does not include experiments.
   - If the paper includes experiments, a No answer to this question will not be perceived well by the reviewers: Making the paper reproducible is important, regardless of whether the code and data are provided or not.
   - If the contribution is a dataset and/or model, the authors should describe the steps taken to make their results reproducible or verifiable.
   - Depending on the contribution, reproducibility can be accomplished in various ways. For example, if the contribution is a novel architecture, describing the architecture fully might suffice, or if the contribution is a specific model and empirical evaluation, it may be necessary to either make it possible for others to replicate the model with the same dataset, or provide access to the model. In general. releasing code and data is often one good way to accomplish this, but reproducibility can also be provided via detailed instructions for how to replicate the results, access to a hosted model (e.g., in the case of a large language model), releasing of a model checkpoint, or other means that are appropriate to the research performed.
   - While NeurIPS does not require releasing code, the conference does require all submissions to provide some reasonable avenue for reproducibility, which may depend on the nature of the contribution. For example
     (a) If the contribution is primarily a new algorithm, the paper should make it clear how to reproduce that algorithm.
     (b) If the contribution is primarily a new model architecture, the paper should describe the architecture clearly and fully.

(c) If the contribution is a new model (e.g., a large language model), then there should either be a way to access this model for reproducing the results or a way to reproduce the model (e.g., with an open-source dataset or instructions for how to construct the dataset).

(d) We recognize that reproducibility may be tricky in some cases, in which case authors are welcome to describe the particular way they provide for reproducibility. In the case of closed-source models, it may be that access to the model is limited in some way (e.g., to registered users), but it should be possible for other researchers to have some path to reproducing or verifying the results.

5. **Open access to data and code**

   Question: Does the paper provide open access to the data and code, with sufficient instructions to faithfully reproduce the main experimental results, as described in supplemental material?

   Answer: [No]

   Justification: Due to time constraints, we were unable to prepare the code for inclusion in the supplementary material. However, we plan to release the full source code upon acceptance. All experiments were conducted on publicly available datasets.

   Guidelines:

   - The answer NA means that paper does not include experiments requiring code.
   - Please see the NeurIPS code and data submission guidelines (`https://nips.cc/public/guides/CodeSubmissionPolicy`) for more details.
   - While we encourage the release of code and data, we understand that this might not be possible, so "No" is an acceptable answer. Papers cannot be rejected simply for not including code, unless this is central to the contribution (e.g., for a new open-source benchmark).
   - The instructions should contain the exact command and environment needed to run to reproduce the results. See the NeurIPS code and data submission guidelines (`https://nips.cc/public/guides/CodeSubmissionPolicy`) for more details.
   - The authors should provide instructions on data access and preparation, including how to access the raw data, preprocessed data, intermediate data, and generated data, etc.
   - The authors should provide scripts to reproduce all experimental results for the new proposed method and baselines. If only a subset of experiments are reproducible, they should state which ones are omitted from the script and why.
   - At submission time, to preserve anonymity, the authors should release anonymized versions (if applicable).
   - Providing as much information as possible in supplemental material (appended to the paper) is recommended, but including URLs to data and code is permitted.

6. **Experimental setting/details**

   Question: Does the paper specify all the training and test details (e.g., data splits, hyperparameters, how they were chosen, type of optimizer, etc.) necessary to understand the results?

   Answer: [Yes]

   Justification: Appendix G provides all experimental settings, including dataset descriptions, evaluation metrics, and the exact hyperparameters used for each experiment.

   Guidelines:

   - The answer NA means that the paper does not include experiments.
   - The experimental setting should be presented in the core of the paper to a level of detail that is necessary to appreciate the results and make sense of them.
   - The full details can be provided either with the code, in appendix, or as supplemental material.

7. **Experiment statistical significance**

   Question: Does the paper report error bars suitably and correctly defined or other appropriate information about the statistical significance of the experiments?

Answer: [Yes]

Justification: We use standard deviation to indicate the spread of results across folds. Table 2 reports mean accuracy and standard deviation computed over 10-fold cross-validation for the node classification task.

Guidelines:

- The answer NA means that the paper does not include experiments.
- The authors should answer "Yes" if the results are accompanied by error bars, confidence intervals, or statistical significance tests, at least for the experiments that support the main claims of the paper.
- The factors of variability that the error bars are capturing should be clearly stated (for example, train/test split, initialization, random drawing of some parameter, or overall run with given experimental conditions).
- The method for calculating the error bars should be explained (closed form formula, call to a library function, bootstrap, etc.)
- The assumptions made should be given (e.g., Normally distributed errors).
- It should be clear whether the error bar is the standard deviation or the standard error of the mean.
- It is OK to report 1-sigma error bars, but one should state it. The authors should preferably report a 2-sigma error bar than state that they have a 96% CI, if the hypothesis of Normality of errors is not verified.
- For asymmetric distributions, the authors should be careful not to show in tables or figures symmetric error bars that would yield results that are out of range (e.g. negative error rates).
- If error bars are reported in tables or plots, The authors should explain in the text how they were calculated and reference the corresponding figures or tables in the text.

8. **Experiments compute resources**

   Question: For each experiment, does the paper provide sufficient information on the computer resources (type of compute workers, memory, time of execution) needed to reproduce the experiments?

   Answer: [Yes]

   Justification: Appendix G provides details on the computing environment, including hardware specifications. Appendix C presents a runtime analysis conducted on the specified hardware.

   Guidelines:

   - The answer NA means that the paper does not include experiments.
   - The paper should indicate the type of compute workers CPU or GPU, internal cluster, or cloud provider, including relevant memory and storage.
   - The paper should provide the amount of compute required for each of the individual experimental runs as well as estimate the total compute.
   - The paper should disclose whether the full research project required more compute than the experiments reported in the paper (e.g., preliminary or failed experiments that didn't make it into the paper).

9. **Code of ethics**

   Question: Does the research conducted in the paper conform, in every respect, with the NeurIPS Code of Ethics `https://neurips.cc/public/EthicsGuidelines`?

   Answer: [Yes]

   Justification: The research conducted in this paper adheres to the NeurIPS Code of Ethics.

   Guidelines:

   - The answer NA means that the authors have not reviewed the NeurIPS Code of Ethics.
   - If the authors answer No, they should explain the special circumstances that require a deviation from the Code of Ethics.

- The authors should make sure to preserve anonymity (e.g., if there is a special consideration due to laws or regulations in their jurisdiction).

10. **Broader impacts**

    Question: Does the paper discuss both potential positive societal impacts and negative societal impacts of the work performed?

    Answer: [NA]

    Justification: The proposed method has no societal impact.

    Guidelines:

    - The answer NA means that there is no societal impact of the work performed.
    - If the authors answer NA or No, they should explain why their work has no societal impact or why the paper does not address societal impact.
    - Examples of negative societal impacts include potential malicious or unintended uses (e.g., disinformation, generating fake profiles, surveillance), fairness considerations (e.g., deployment of technologies that could make decisions that unfairly impact specific groups), privacy considerations, and security considerations.
    - The conference expects that many papers will be foundational research and not tied to particular applications, let alone deployments. However, if there is a direct path to any negative applications, the authors should point it out. For example, it is legitimate to point out that an improvement in the quality of generative models could be used to generate deepfakes for disinformation. On the other hand, it is not needed to point out that a generic algorithm for optimizing neural networks could enable people to train models that generate Deepfakes faster.
    - The authors should consider possible harms that could arise when the technology is being used as intended and functioning correctly, harms that could arise when the technology is being used as intended but gives incorrect results, and harms following from (intentional or unintentional) misuse of the technology.
    - If there are negative societal impacts, the authors could also discuss possible mitigation strategies (e.g., gated release of models, providing defenses in addition to attacks, mechanisms for monitoring misuse, mechanisms to monitor how a system learns from feedback over time, improving the efficiency and accessibility of ML).

11. **Safeguards**

    Question: Does the paper describe safeguards that have been put in place for responsible release of data or models that have a high risk for misuse (e.g., pretrained language models, image generators, or scraped datasets)?

    Answer: [NA]

    Justification: The paper poses no such risks.

    Guidelines:

    - The answer NA means that the paper poses no such risks.
    - Released models that have a high risk for misuse or dual-use should be released with necessary safeguards to allow for controlled use of the model, for example by requiring that users adhere to usage guidelines or restrictions to access the model or implementing safety filters.
    - Datasets that have been scraped from the Internet could pose safety risks. The authors should describe how they avoided releasing unsafe images.
    - We recognize that providing effective safeguards is challenging, and many papers do not require this, but we encourage authors to take this into account and make a best faith effort.

12. **Licenses for existing assets**

    Question: Are the creators or original owners of assets (e.g., code, data, models), used in the paper, properly credited and are the license and terms of use explicitly mentioned and properly respected?

    Answer: [Yes]

Justification: We ensure proper attribution to the original papers and owners of all external data, code, and models utilized in this work.

Guidelines:

- The answer NA means that the paper does not use existing assets.
- The authors should cite the original paper that produced the code package or dataset.
- The authors should state which version of the asset is used and, if possible, include a URL.
- The name of the license (e.g., CC-BY 4.0) should be included for each asset.
- For scraped data from a particular source (e.g., website), the copyright and terms of service of that source should be provided.
- If assets are released, the license, copyright information, and terms of use in the package should be provided. For popular datasets, `paperswithcode.com/datasets` has curated licenses for some datasets. Their licensing guide can help determine the license of a dataset.
- For existing datasets that are re-packaged, both the original license and the license of the derived asset (if it has changed) should be provided.
- If this information is not available online, the authors are encouraged to reach out to the asset's creators.

13. **New assets**

Question: Are new assets introduced in the paper well documented and is the documentation provided alongside the assets?

Answer: [Yes]

Justification: The documentation of our source code will be provided alongside the code, upon acceptance.

Guidelines:

- The answer NA means that the paper does not release new assets.
- Researchers should communicate the details of the dataset/code/model as part of their submissions via structured templates. This includes details about training, license, limitations, etc.
- The paper should discuss whether and how consent was obtained from people whose asset is used.
- At submission time, remember to anonymize your assets (if applicable). You can either create an anonymized URL or include an anonymized zip file.

14. **Crowdsourcing and research with human subjects**

Question: For crowdsourcing experiments and research with human subjects, does the paper include the full text of instructions given to participants and screenshots, if applicable, as well as details about compensation (if any)?

Answer: [NA]

Justification: The paper does not involve crowdsourcing nor research with human subjects.

Guidelines:

- The answer NA means that the paper does not involve crowdsourcing nor research with human subjects.
- Including this information in the supplemental material is fine, but if the main contribution of the paper involves human subjects, then as much detail as possible should be included in the main paper.
- According to the NeurIPS Code of Ethics, workers involved in data collection, curation, or other labor should be paid at least the minimum wage in the country of the data collector.

15. **Institutional review board (IRB) approvals or equivalent for research with human subjects**

Question: Does the paper describe potential risks incurred by study participants, whether such risks were disclosed to the subjects, and whether Institutional Review Board (IRB) approvals (or an equivalent approval/review based on the requirements of your country or institution) were obtained?

Answer: [NA]

Justification: The paper does not involve crowdsourcing nor research with human subjects.

Guidelines:

- The answer NA means that the paper does not involve crowdsourcing nor research with human subjects.
- Depending on the country in which research is conducted, IRB approval (or equivalent) may be required for any human subjects research. If you obtained IRB approval, you should clearly state this in the paper.
- We recognize that the procedures for this may vary significantly between institutions and locations, and we expect authors to adhere to the NeurIPS Code of Ethics and the guidelines for their institution.
- For initial submissions, do not include any information that would break anonymity (if applicable), such as the institution conducting the review.

16. **Declaration of LLM usage**

Question: Does the paper describe the usage of LLMs if it is an important, original, or non-standard component of the core methods in this research? Note that if the LLM is used only for writing, editing, or formatting purposes and does not impact the core methodology, scientific rigorousness, or originality of the research, declaration is not required.

Answer: [NA]

Justification: The core method development in this research does not involve LLMs.

Guidelines:

- The answer NA means that the core method development in this research does not involve LLMs as any important, original, or non-standard components.
- Please refer to our LLM policy (`https://neurips.cc/Conferences/2025/LLM`) for what should or should not be described.

A Appendix - Theorems' proofs

A.1 Proof of Proposition 3.2

[Proof of Proposition 3.2] Given a graph $\mathcal{G}$ with a graph Laplacian $\boldsymbol{L}$ and its coarsened graph $\mathcal{G}_c$ with a graph Laplacian $\boldsymbol{L}_c = \boldsymbol{C}^T\boldsymbol{L}\boldsymbol{C}$, and assume that for any two graph signals $\boldsymbol{x}, \boldsymbol{y} \in \mathbb{R}^n$, the following condition is satisfied:

$$\boldsymbol{x}^\top \boldsymbol{L}\boldsymbol{y} = \boldsymbol{x}_c^\top \boldsymbol{L}_c \boldsymbol{y}_c \tag{11}$$

We plug in the the definitions of $\boldsymbol{x}_c = \boldsymbol{P}\boldsymbol{x}$ and $\boldsymbol{y}_c = \boldsymbol{P}\boldsymbol{y}$ in (11) and obtain:

$$\begin{aligned}\boldsymbol{x}^\top \boldsymbol{L}\boldsymbol{y} &= \boldsymbol{x}_c^\top \boldsymbol{L}_c \boldsymbol{y}_c \\ &= (\boldsymbol{P}\boldsymbol{x})^\top \boldsymbol{L}_c \boldsymbol{P}\boldsymbol{y} \\ &= \boldsymbol{x}^\top \boldsymbol{P}^\top \boldsymbol{L}_c \boldsymbol{P}\boldsymbol{y} \\ &= \boldsymbol{x}^\top \boldsymbol{L}_l \boldsymbol{y}. \end{aligned} \tag{12}$$

where in the last equality we plug-in the definition of the lifted Laplacian (reconstructed Laplacian) $\boldsymbol{L}_l = \boldsymbol{P}^T\boldsymbol{L}_c\boldsymbol{P}$.

Assuming (12) holds for every pair of signals $\boldsymbol{x}, \boldsymbol{y} \in \mathbb{R}^n$, one can choose specific signals such that $\boldsymbol{L}[i,j] = \boldsymbol{L}_l[i,j]$ for all $i, j = 1, \ldots, n$, allowing us to conclude:

$$\boldsymbol{L} = \boldsymbol{L}_l$$

This implies that the full Laplacian $\boldsymbol{L}$ can be fully reconstructed for $\boldsymbol{L}_c$.

A.2 Proof of Proposition 3.4

[Proof of Proposition 3.4] Let $\boldsymbol{x}, \boldsymbol{y} \in \mathbb{R}^n$ be two k-smooth signals on the graph $\mathcal{G}$ with graph Laplacian $\boldsymbol{L}$. Define $\boldsymbol{x}_c = \boldsymbol{C}^\top \boldsymbol{x}, \boldsymbol{y}_c = \boldsymbol{C}^\top \boldsymbol{y} \in \mathbb{R}^k$, and let $\boldsymbol{L}_c = \boldsymbol{C}^\top \boldsymbol{L}\boldsymbol{C}$, where $\boldsymbol{C} = \boldsymbol{U}^{(k)}\boldsymbol{O}$, and $\boldsymbol{O} \in \mathcal{O}$ is some k-dimension rotation matrix. Then, the following relation holds:

$$\begin{aligned}\boldsymbol{x}^\top \boldsymbol{L}\boldsymbol{y} - \boldsymbol{x}_c^\top \boldsymbol{L}_c \boldsymbol{y}_c &= \boldsymbol{x}^\top \boldsymbol{L}\boldsymbol{y} - ((\boldsymbol{C}^\top \boldsymbol{x})^\top \boldsymbol{C}^\top \boldsymbol{L}\boldsymbol{C}\boldsymbol{C}^\top \boldsymbol{y} \\ &= \boldsymbol{x}^\top \boldsymbol{L}\boldsymbol{y} - ((\boldsymbol{U}^{(k)}\boldsymbol{O})^\top \boldsymbol{x})^\top (\boldsymbol{U}^{(k)}O)^\top \boldsymbol{L}\boldsymbol{U}^{(k)}\boldsymbol{O}(\boldsymbol{U}^{(k)}\boldsymbol{O})^\top \boldsymbol{y} \\ &= \boldsymbol{x}^\top \boldsymbol{L}\boldsymbol{y} - \boldsymbol{x}^\top \boldsymbol{U}^{(k)}\boldsymbol{O}\boldsymbol{O}^\top (\boldsymbol{U}^{(k)})^\top \boldsymbol{L}\boldsymbol{U}^{(k)}\boldsymbol{O}\boldsymbol{O}^\top (\boldsymbol{U}^{(k)})^\top \boldsymbol{y} \\ &= \boldsymbol{x}^\top \boldsymbol{L}\boldsymbol{y} - \boldsymbol{x}^\top \boldsymbol{U}^{(k)} (\boldsymbol{U}^{(k)})^\top L \boldsymbol{U}^{(k)} (\boldsymbol{U}^{(k)})^\top \boldsymbol{y} \\ &= \boldsymbol{x}^\top \boldsymbol{L}\boldsymbol{y} - \boldsymbol{x}^\top \boldsymbol{L}\boldsymbol{y} = 0 \end{aligned}$$

where the third equality holds because $\boldsymbol{O}$ is a rotation matrix satisfying $\boldsymbol{O}\boldsymbol{O}^\top = \boldsymbol{I}_{k\times k}$. The fifth equality holds because $\boldsymbol{x}$ and $\boldsymbol{y}$ are k-smooth and satisfy $\boldsymbol{x} = \boldsymbol{U}^{(k)}(\boldsymbol{U}^{(k)})^\top \boldsymbol{x}$ and $\boldsymbol{y} = \boldsymbol{U}^{(k)}(\boldsymbol{U}^{(k)})^\top \boldsymbol{y}$.

Thus, for any matrix $\boldsymbol{X}$ whose columns are k-smooth signals, we have:

$$\|\boldsymbol{X}^\top \boldsymbol{L}\boldsymbol{X} - \boldsymbol{X}_c^\top \boldsymbol{L}_c \boldsymbol{X}_c\|_F^2 = 0.$$

A.3 Proof of Proposition 3.5

The proof of Proposition 3.5 relies on the following definition and lemma.

Definition A.1 (Restricted spectral approximation [10]) *Let R be a k-dimensional subspace of $\mathbb{R}^n$. Matrices $\boldsymbol{L}_c$ and $\boldsymbol{L}$ are (R, ϵ)-similar if there exists an $\epsilon > 0$ such that*

$$\|\boldsymbol{x} - \boldsymbol{x}_l\|_L \leq \epsilon \|\boldsymbol{x}\|_L, \quad \textit{for all } \boldsymbol{x} \in R,$$

where $\boldsymbol{x}_l = \boldsymbol{C}\boldsymbol{C}^\dagger \boldsymbol{x}$.

Lemma A.2 *Let $\boldsymbol{L}$ be the Laplacian matrix of a connected graph $\mathcal{G}$, and let $\boldsymbol{U}^{(k)}$ be the matrix containing its k-leading eigenvectors. Suppose $\boldsymbol{L}_c = \boldsymbol{C}^\top \boldsymbol{L}\boldsymbol{C}$ is the Laplacian matrix of a coarsened graph derived using a coarsening operator $\boldsymbol{C}$ with normalized columns such that*

$$tr(\boldsymbol{U}^{(k)}(\boldsymbol{U}^{(k)})^\top \boldsymbol{C}\boldsymbol{C}^\top) = k - \epsilon.$$

Then, the matrices $\boldsymbol{L}$ and $\boldsymbol{L}_c$ are $(R, \epsilon\kappa)$-similar, where $\kappa = \frac{\lambda_{max}(\boldsymbol{L})}{\lambda_2(\boldsymbol{L})}$, and $R = span(\boldsymbol{U}^{(k)})$

[Proof of Lemma A.2] We note the projection matrix defined by $\boldsymbol{C}$ as $\boldsymbol{\Pi}_C = \boldsymbol{C}\boldsymbol{C}^\top$. Given the trace condition $\text{tr}(\boldsymbol{U}^{(k)}(\boldsymbol{U}^{(k)})^\top \boldsymbol{\Pi}_C) = k - \epsilon$, we can express it as:

$$\text{tr}(\boldsymbol{U}^{(k)}(\boldsymbol{U}^{(k)})^\top \boldsymbol{\Pi}_C) = \text{tr}((\boldsymbol{U}^{(k)})^\top \boldsymbol{\Pi}_C \boldsymbol{U}^{(k)}) = k - \epsilon.$$

From this, we immediately obtain:

$$\text{tr}((\boldsymbol{U}^{(k)})^\top (\boldsymbol{I} - \boldsymbol{\Pi}_C)\boldsymbol{U}^{(k)}) = \epsilon. \tag{13}$$

This follows from the fact that:

$$\begin{aligned} k &= \text{tr}((\boldsymbol{U}^{(k)})^\top \boldsymbol{U}^{(k)}) = \text{tr}(\boldsymbol{U}^{(k)}(\boldsymbol{U}^{(k)})^\top) = \text{tr}(\boldsymbol{U}^{(k)} \boldsymbol{I}_{n\times n} \boldsymbol{U}^{(k)}) \\ &= \text{tr}((\boldsymbol{U}^{(k)})^\top \boldsymbol{\Pi}_C \boldsymbol{U}^{(k)}) + \text{tr}((\boldsymbol{U}^{(k)})^\top (\boldsymbol{I} - \boldsymbol{\Pi}_C)\boldsymbol{U}^{(k)}), \end{aligned}$$

where the first equality holds because $\boldsymbol{U}^{(k)}$ is orthonormal matrix.

Next, we express the term $\|\boldsymbol{x} - \boldsymbol{x}_l\|_L$. Since the columns of $\boldsymbol{C}$ are orthogonal, we can use $\boldsymbol{x}_l = \boldsymbol{C}\boldsymbol{P}\boldsymbol{x} = \boldsymbol{C}\boldsymbol{C}^\dagger \boldsymbol{x} = \boldsymbol{C}\boldsymbol{C}^\top \boldsymbol{x}$, and obtain:

$$\begin{aligned} \|\boldsymbol{x} - \boldsymbol{x}_l\|_L &= (\boldsymbol{x} - \boldsymbol{C}\boldsymbol{C}^\top \boldsymbol{x})^\top \boldsymbol{L}(\boldsymbol{x} - \boldsymbol{C}\boldsymbol{C}^\top \boldsymbol{x}) \\ &= ((\boldsymbol{I} - \boldsymbol{C}\boldsymbol{C}^\top)\boldsymbol{x})^\top \boldsymbol{L}(\boldsymbol{I} - \boldsymbol{C}\boldsymbol{C}^\top)\boldsymbol{x}. \end{aligned} \tag{14}$$

Using the Rayleigh quotient [39], we can bound by:

$$\begin{aligned} \|\boldsymbol{x} - \boldsymbol{x}_l\|_L &= ((\boldsymbol{I} - \boldsymbol{C}\boldsymbol{C}^\top)\boldsymbol{x})^\top \boldsymbol{L}((\boldsymbol{I} - \boldsymbol{C}\boldsymbol{C}^\top)\boldsymbol{x}) \\ &\leq \lambda_{\max}(\boldsymbol{L})\|(\boldsymbol{I} - \boldsymbol{C}\boldsymbol{C}^\top)\boldsymbol{x}\|_2^2. \end{aligned} \tag{15}$$

Next, we proceed to bound the term $\|(\boldsymbol{I} - \boldsymbol{C}\boldsymbol{C}^\top)\boldsymbol{x}\|_2^2$. Since $\boldsymbol{x}$ is spanned by $\boldsymbol{U}^{(k)}$, we write $\boldsymbol{x} = \boldsymbol{U}^{(k)}\boldsymbol{z}$. Therefore, we get:

$$\|(\boldsymbol{I} - \boldsymbol{C}\boldsymbol{C}^\top)\boldsymbol{x}\|_2^2 = \boldsymbol{z}^\top (\boldsymbol{U}^{(k)})^\top (\boldsymbol{I} - \boldsymbol{C}\boldsymbol{C}^\top)\boldsymbol{U}^{(k)}\boldsymbol{z}.$$

From (13), we know that the maximum eigenvalue of $(\boldsymbol{U}^{(k)})^\top (\boldsymbol{I} - \boldsymbol{\Pi}_C)\boldsymbol{U}^{(k)}$ is bounded by ϵ. Thus, by applying the Rayleigh quotient, we obtain:

$$\|(\boldsymbol{I} - \boldsymbol{C}\boldsymbol{C}^\top)\boldsymbol{x}\|_2^2 \leq \epsilon\|\boldsymbol{z}\|_2^2 = \epsilon\|\boldsymbol{x}\|_2^2.$$

Substituting this bound into (15), we have:

$$\|\boldsymbol{x} - \boldsymbol{x}_l\|_L \leq \epsilon\lambda_{\max}(\boldsymbol{L})\|\boldsymbol{x}\|_2^2.$$

Since $\boldsymbol{L}$ is the graph Laplacian of a connected graph, it has only one zero eigenvalue, corresponding to the constant vector. Assuming $\boldsymbol{x}$ is not a constant vector, we can bound $\|\boldsymbol{x}\|_2^2$ using the Rayleigh quotient:

$$\|\boldsymbol{x}\|_2^2 \geq \frac{\|\boldsymbol{x}\|_L}{\lambda_2(\boldsymbol{L})}.$$

Substituting this into the previous inequality, we obtain:

$$\|\boldsymbol{x} - \boldsymbol{x}_l\|_L \leq \epsilon \frac{\lambda_{\max}(\boldsymbol{L})}{\lambda_2(\boldsymbol{L})} \|\boldsymbol{x}\|_L = \epsilon\kappa \|\boldsymbol{x}\|_L,$$

where $\kappa = \frac{\lambda_{\max}(\boldsymbol{L})}{\lambda_2(\boldsymbol{L})}$ is the condition number of $\boldsymbol{L}$.

Finally, if $\boldsymbol{x}$ is a constant vector, then since the columns of $\boldsymbol{C}$ span the constant vector, we have:

$$\|\boldsymbol{x} - \boldsymbol{x}_l\|_L = \|\boldsymbol{x} - \boldsymbol{C}\boldsymbol{C}^\top \boldsymbol{x}\|_L = 0.$$

Thus, for all $\boldsymbol{x} \in \text{span}(\boldsymbol{U}^{(k)})$, we conclude that:

$$\|\boldsymbol{x} - \boldsymbol{x}_l\|_L \leq \epsilon\kappa \|\boldsymbol{x}\|_L.$$

i.e $\boldsymbol{L}$ and $\boldsymbol{L}_c$ are $(R, \epsilon\kappa)$ similar.

Then, according to Theorem 13 and Corollary 12 in [20], if the full graph Laplacian $\boldsymbol{L}$ and the coarsen graph Laplacian are $\boldsymbol{L}_c$ are $(\boldsymbol{U}^{(k)}, \epsilon\kappa)$-similar, they satisfy the following inequalities: :

$$(1 - \epsilon\kappa)\|\boldsymbol{x}\|_L \leq \|\boldsymbol{x}|_{L_c} \leq (1 + \epsilon\kappa)\|\boldsymbol{x}\|_L$$

$$\frac{1}{\mu_1}\lambda^{(i)} \leq \lambda_c^{(i)} \leq \frac{1}{\mu_2} \frac{(1 + \epsilon\kappa)^2}{1 - (\epsilon\kappa)^2(\lambda^{(i)}/\lambda^{(2)})}\lambda^{(i)}, \qquad 2 \leq i \leq k$$

according to Proposition 3.5, where $\kappa = \frac{\lambda_{\max}(\boldsymbol{L})}{\lambda_2(\boldsymbol{L})}$, and μ_1,μ_2 and the first and k eigenvalues of the matrix $\boldsymbol{P}\boldsymbol{P}^\top$.

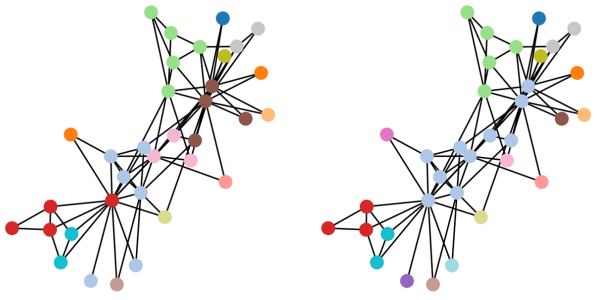

(a) (b)

Figure 2: Clustering of the Karate Club network using (a) our SINGC method and (b) conventional k-means clustering on the leading eigenvectors. Each color represents a distinct cluster, and the coarsened graph is obtained by mapping nodes from the same cluster (color) to a single super-node. We observe that the clusters produced by SINGC are more balanced, which is advantageous for downstream graph learning tasks.

A.4 Gradient Computation

We start with a recap of our suggested objective function:

$$\begin{aligned}\min_{\boldsymbol{X}_c, \boldsymbol{C}} f(\boldsymbol{X}_c, \boldsymbol{C}) = \|\boldsymbol{X}^\top \boldsymbol{L}\boldsymbol{X} - \boldsymbol{X}_c^\top \boldsymbol{C}^\top \boldsymbol{L}\boldsymbol{C}\boldsymbol{X}_c\|_F - \beta tr(\boldsymbol{U}^{(k)}(\boldsymbol{U}^{(k)})^\top \boldsymbol{C}\boldsymbol{C}^\top) \\ + \lambda\|\boldsymbol{C}^T\|_{1,2}^2 - \alpha \log\det(\boldsymbol{L}_c + \boldsymbol{J}) \\ \textbf{s.t.} \qquad \boldsymbol{X}_c = \boldsymbol{C}^\dagger \boldsymbol{X}\end{aligned}$$

The gradient of each term with respect to C is:

$$\begin{aligned}
\nabla_{\boldsymbol{C}}(-tr(\boldsymbol{U}^{(k)}(\boldsymbol{U}^{(k)})^\top \boldsymbol{C}\boldsymbol{C}^\top)) &= -2\boldsymbol{U}^{(k)}(\boldsymbol{U}^{(k)})^\top \boldsymbol{C} \\
\nabla_{\boldsymbol{C}}(\|\boldsymbol{X}^\top \boldsymbol{L}\boldsymbol{X} - \boldsymbol{X}_c^\top \boldsymbol{C}^\top \boldsymbol{L}\boldsymbol{C}\boldsymbol{X}_c\|_F) &= -(2\boldsymbol{L}\boldsymbol{C}\boldsymbol{X}_c(\boldsymbol{X}^\top \boldsymbol{L}\boldsymbol{X} - (\boldsymbol{L}\boldsymbol{C}\boldsymbol{X}_c)^\top \boldsymbol{C}\boldsymbol{X}_c)\boldsymbol{X}_c^\top \\
&\quad + 2\boldsymbol{L}^\top \boldsymbol{C}\boldsymbol{X}_c(\boldsymbol{X}^\top \boldsymbol{L}\boldsymbol{X} - (\boldsymbol{C}\boldsymbol{X}_c)^\top \boldsymbol{L}\boldsymbol{C}\boldsymbol{X}_c)\boldsymbol{X}_c^\top) \\
\nabla_{\boldsymbol{C}}(\|\boldsymbol{C}^T\|_{1,2}^2) &= \boldsymbol{C}\boldsymbol{1}_{k\times k} \\
\nabla_{\boldsymbol{C}}(logdet(\boldsymbol{L}_c + \boldsymbol{J})) &= \boldsymbol{L}\boldsymbol{C}(\boldsymbol{C}^\top \boldsymbol{L}\boldsymbol{C} + \boldsymbol{J})^{-1}
\end{aligned}$$

where the third was shown in [14], assuming all elements of $\boldsymbol{C}$ to non-negative (since $\boldsymbol{C} \in \mathcal{C}$. The full gradient with respect to $\boldsymbol{C}$ of (9) is:

$$\begin{aligned}
\nabla_{\boldsymbol{C}} f(\boldsymbol{C}, \boldsymbol{X}_c) &= 2\beta\boldsymbol{U}^{(k)}(\boldsymbol{U}^{(k)})^\top \boldsymbol{C} + \lambda\boldsymbol{C} \\
&\quad - (2\boldsymbol{L}\boldsymbol{C}\boldsymbol{X}_c(\boldsymbol{X}^\top \boldsymbol{L}\boldsymbol{X} - (\boldsymbol{L}\boldsymbol{C}\boldsymbol{X}_c)^\top \boldsymbol{C}\boldsymbol{X}_c)\boldsymbol{X}_c^\top \\
&\quad + 2\boldsymbol{L}^\top \boldsymbol{C}\boldsymbol{X}_c(\boldsymbol{X}^\top \boldsymbol{L}\boldsymbol{X} - (\boldsymbol{C}\boldsymbol{X}_c)^\top \boldsymbol{L}\boldsymbol{C}\boldsymbol{X}_c)\boldsymbol{X}_c^\top) \\
&\quad + \lambda\boldsymbol{C}\boldsymbol{1}_{k\times k} - \alpha(\boldsymbol{L}\boldsymbol{C}(\boldsymbol{C}^\top \boldsymbol{L}\boldsymbol{C} + \boldsymbol{J})^{-1})
\end{aligned} \tag{16}$$

We note that in case of the SINGC Algorithm the computed gradient is simpler and can be express as:

$$\nabla_{\boldsymbol{C}} \tilde{f}(\boldsymbol{C}, \boldsymbol{X}_c) = 2\boldsymbol{U}^{(k)}(\boldsymbol{U}^{(k)})^\top \boldsymbol{C} + \lambda\boldsymbol{C}\boldsymbol{1}_{k\times k} - \alpha(\boldsymbol{L}\boldsymbol{C}(\boldsymbol{C}^\top \boldsymbol{L}\boldsymbol{C} + \boldsymbol{J})^{-1}) \tag{17}$$

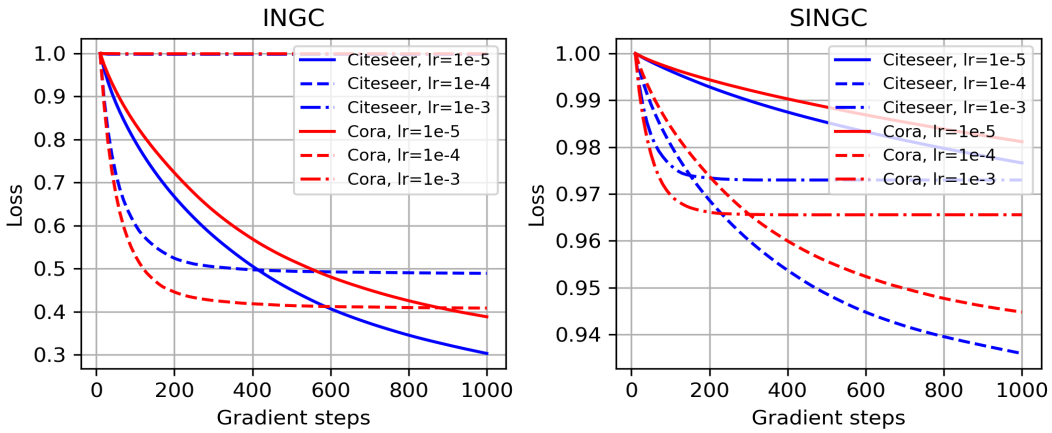

Figure 3: Convergence rates of INGC and SINGC methods for Cora and Citeseer datasets. Citeseer results are shown in blue with varying line styles for different learning rates, while Cora results are shown in red. Gradient steps are on the x-axis, and normalized loss values are on the y-axis.

B Methods Performance - Visual Comparison

Table 3: Comparison of gradient expressions and time complexities for FGC, INGC, and SINGC.

	FGC	**INGC**	**SINGC**
Gradient Expression	$\nabla_C f(C, X_c) = 2\big((CX_c - X) + L(CX_c)\big)X_c^\top + \lambda C\mathbf{1}_{k\times k} - \alpha\big(LC(C^\top LC + J)^{-1}\big)$	$\nabla_C f(C, X_c) = 2\beta U^{(k)}(U^{(k)})^\top C - \big[2L(CX_c)\big(X^\top LX - (LCX_c)^\top (CX_c)\big)X_c^\top\big] + \lambda C\mathbf{1}_{k\times k} - \alpha\big(LC(C^\top LC + J)^{-1}\big)$	$\nabla_C f(C) = 2U^{(k)}(U^{(k)})^\top C + \lambda C\mathbf{1}_{k\times k} - \alpha\big(LC(C^\top LC + J)^{-1}\big)$
Theoretical Time Complexity	$O\big(n^2(k+d) + k^3\big)$	$O\big(n^2(k+d) + ndk + nk^2 + k^3\big)$	$O\big(n^2k + nk^2 + k^3\big)$

In Section 4, we demonstrated the global preservation property of our method on a specific task with a low number of super-nodes, similar to a clustering task. However, in typical coarsening scenarios,

Table 4: Runtime comparison of our methods and FGC for a coarsening ratio of $r = 0.03$, where all times τ are reported in seconds. Columns 2–5 show the runtime of each coarsening algorithm. Column 6 reports the training time of a GCN on the original graph, while Column 7 reports the training time on the coarsened graph. The final column shows in percentage how much training time was saved by applying coarsening before training, compared to training on the full graph.

Dataset	FGC	INGC	SINGC	INGC($\beta = 0$)	GCN full	GCN coarse	Speedup
Citeseer	04.67	09.38	04.04	06.11	42.02	26.03	14-29%
Pubmed	20.54	75.27	49.47	33.05	93.15	23.92	21-38%
Co-CS	70.80	284.13	180.33	120.66	369.10	40.86	12-56%
Co-Phy	266.83	1200.76	720.22	540.50	883.96	52.26	12-32%

there are usually a larger number of super-nodes. In this section, we present the performance of this property in more practical coarsening scenarios, showing how our method continues to preserve the global structure of the graph.

In Figures 5 and 7 , we present the results obtained by our methods (INGC/SINGC), alongside the three baseline methods described in Section 4 on the Karate Club and Les Miserables datasets. Each row in the figures shows the partitioning produced by each method at different coarsening ratios. Nodes of the same color are grouped into the same super-node. We observe that our method groups adjacent nodes into super-nodes, thereby preserving the global structure of the graph.

Since our method leverages the graph Laplacian eigenvectors to partition the vertices, we also compare it to the commonly used spectral clustering approach [19], which partitions the vertices by applying k-means [40] on the leading graph Laplacian eigenvectors. In Figure 2, we present the clustering results obtained by the SINGC method on the well-known Karate Club dataset[31], which consists of $n = 34$ nodes. We apply our method with a target of $k = \frac{n}{2} = 17$ super-nodes and compare the results to those obtained by spectral clustering[19] applied to the top k leading eigenvectors. In the figure, each color represents a distinct cluster.We observe that the clusters produced by our method are more balanced compared to those generated by spectral clustering, which tends to form one large cluster alongside several smaller, single-node clusters. This balance is advantageous for downstream graph learning tasks, such as graph pooling.

C Complexity Analysis

For an input graph with n nodes, e edges, and node features of dimension p, the coarsened graph has k nodes and e_c edges. The dominant computational cost of the coarsening process arises from the gradient computation performed at each optimization step. Table 3 summarizes the gradient expressions and their time complexities, highlighting that SINGC is the most efficient, while INGC remains competitive with FGC, considering the gradient computation.

Both INGC and SINGC have additional overhead beyond the optimization itself due to the computation of the top-k Laplacian eigenvectors, which typically requires $\mathcal{O}(n^2k)$ operations. This step can significantly increase the total runtime. However, this cost can be avoided by setting $\beta = 0$, which removes the Grassmann similarity term from the objective. As shown in Table 6, even without this term, our methods still outperform the baselines.

Table 4 reports the runtime of our methods and FGC, demonstrating their efficiency in reducing GNN training time. Specifically, we compare the time required to train a GCN on the original graph versus the coarse graph, including the coarsening time. The results confirm that applying coarsening before GCN training yields substantial time savings as summarized in the last column of the Table.

All runtime values are reported in seconds. Experiments were conducted on a machine with a 12th-Gen Intel i7 CPU, an NVIDIA RTX A5000 GPU, and 64 GB of RAM.

Table 5: Average fraction of signal energy captured by the first k Laplacian eigenvectors (i.e., k-smoothness) for each dataset and coarsening ratio.

Dataset	r=1	r=0.7	r=0.5	r=0.3	r=0.1	r=0.05	r=0.03	r=0.01
Cora	1	0.85	0.74	0.60	0.38	0.27	0.19	0.08
Citeseer	1	0.86	0.76	0.63	0.34	0.25	0.18	0.10
Pubmed	1	0.87	0.77	0.65	0.50	0.43	0.39	0.32
Co-CS	1	0.77	0.67	0.55	0.34	0.26	0.22	0.14

D Convergence Analysis

Figure 3 illustrates the convergence rates of the INGC and SINGC methods on the Cora dataset for a coarsening ratio $r = 0.3$. The left subplot shows the performance of INGC, while the right subplot depicts SINGC. For both methods, Citeseer results are in blue with varying line styles for different learning rates, and Cora results in red with corresponding line styles. The x-axis represents gradient steps, and the y-axis shows normalized loss values.

The results reveal a typical convergence pattern for different learning rates. A trade-off is observed between convergence speed and final objective loss: higher learning rates lead to faster convergence but result in a higher final loss. This phenomenon is consistent across both datasets. We note that recent work has shown that lower learning rates can achieve lower minimal loss values but may risk unstable solutions [41].

E Smoothness Assumption

Assumption 3.3 is a standard premise in graph signal processing and learning on graphs, closely related to the notion of homogeneity and homophily in datasets [42]. To assess how frequently this assumption holds in practice, we evaluate the k-smoothness of node features by computing the fraction of their energy captured by the subspace spanned by the first k Laplacian eigenvectors. Table 5 reports the average energy concentration across all datasets used in our experiments for various values of k.

Notably, our method performs well even when the smoothness assumption is only partially satisfied. This highlights its robustness and broader applicability beyond the ideal smooth setting.

F Hyperparameters Discussion and Ablation Study

We review the purpose of each term in our optimization and clarify the motivations behind selecting the hyperparameters values. The parameter β promotes minimizing the IPE for general smooth signals. As shown in Proposition 3, minimizing the respective term also bounds the REE (related to preserving the graph's global structure) and DE (related to preserving the norm of node features). Therefore, β is significant when these properties are prioritized in coarsening. The parameter λ enforces group sparsity in each row, ensuring the validity of the obtained coarsening operator C. Since C lacks meaningful structure without this term, we did not perform an ablation study on λ. Finally, the parameter α promotes connectivity in the coarsened graph, making it significant in scenarios where preserving graph connectivity is essential.

Figure 4 presents an experiment analyzing each parameter's contribution and our method's sensitivity to their variations. The bars represent normalized scores for different values of a given hyperparameter, with distinct colors denoting specific values. For all metrics, lower values indicate better performance. The other two parameters are set to their optimal values for each metric as specified in Table 9. The figure illustrates the sensitivity of each parameter and evaluates the impact of deviations from optimal values on various metrics.

In Figures 4(a) and 4(b), varying α shows minimal sensitivity across metrics, except for IPE, where changes up to an order of magnitude still yield similar results. Additionally, the figures include an ablation study on the parameter α illustrating its contribution to the optimization process. In Figures 4(c) and 4(d), varying λ demonstrates that our methods are more sensitive to this parameter, highlighting its critical role in performance.

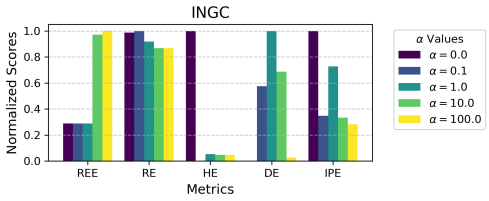

(a) Sensitivity to α (INGC)

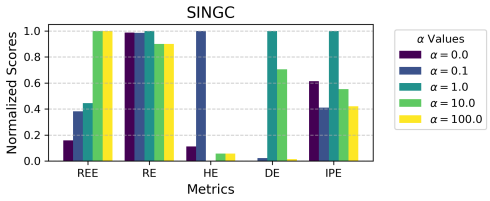

(b) Sensitivity to α (SINGC)

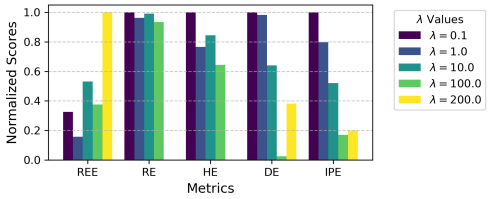

(c) Sensitivity to λ (INGC)

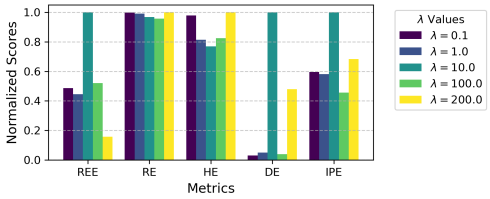

(d) Sensitivity to λ (SINGC)

Figure 4: Ablation study on the sensitivity and contribution of the hyperparameters α and λ across different metrics on the Cora dataset with a coarsening ratio $r = 0.3$. (a) and (b) show the sensitivity of the parameter α across metrics. (c) and (d) illustrate the sensitivity of the methods to parameter λ. The bars represent normalized scores for different values of the respective hyperparameter, with distinct colors denoting specific values. Lower bar values indicate better performance.

Table 6: Ablation study of the parameter β on node classification tasks. The table reports the accuracy on various datasets for different coarsening ratios r using different coarsening methods. The third column presents the results of our INGC method with $\beta = 0$, the fourth column corresponds to the optimal β value, and the fifth column shows the results of SINGC. Best results are in bold; second-best results are underlined. The last two rows indicate the number of times each method achieved the best and second-best performance.

Dataset	r	INGC($\beta = 0$)	INGC	SINGC
Cora	0.3	84.62 ± 0.59	$\mathbf{87.55 \pm 0.16}$	84.51 ± 0.33
	0.1	83.01 ± 0.53	$\mathbf{83.38 \pm 0.47}$	82.76 ± 0.32
	0.05	76.92 ± 1.11	77.42 ± 0.78	$\mathbf{77.81 \pm 0.68}$
Citeseer	0.3	76.25 ± 0.28	$\mathbf{76.89 \pm 0.23}$	76.66 ± 0.27
	0.1	67.07 ± 0.59	$\mathbf{72.63 \pm 0.25}$	69.71 ± 0.72
	0.05	60.66 ± 1.58	66.02 ± 0.32	$\mathbf{66.37 \pm 0.57}$
Pubmed	0.05	$\mathbf{83.60 \pm 0.23}$	$\mathbf{83.59 \pm 0.22}$	83.55 ± 0.32
	0.03	81.62 ± 0.14	81.93 ± 0.22	$\mathbf{83.19 \pm 0.18}$
	0.01	79.08 ± 0.72	79.09 ± 0.26	$\mathbf{79.96 \pm 0.34}$
Co-CS	0.05	90.42 ± 0.18	90.84 ± 0.12	$\mathbf{90.92 \pm 0.22}$
	0.03	89.28 ± 0.21	89.59 ± 0.38	$\mathbf{89.99 \pm 0.41}$
	0.01	77.79 ± 1.15	$\mathbf{87.93 \pm 0.33}$	83.39 ± 0.33
#Best		1	6	6
#2-Best		1	6	5

In Table 6, we present an ablation study on the parameter β for the node classification task across various datasets and coarsening ratios r. The comparison includes three methods: INGC with $\beta = 0$ (ignoring the term $\text{tr}(U^{(k)}(U^{(k)})^\top CC^\top)$ for minimizing IPE for general smooth signals), INGC with the optimal β, and SINGC (our second proposed method, which omits the first term of the objective entirely). The table reports node classification accuracy, with the best results highlighted in bold and the second-best results underlined. For each metric, other hyperparameters are set to their optimal values. The results demonstrate the importance of balancing the two complementary approaches to minimizing IPE. INGC with $\beta = 0$ generally underperforms compared to the other methods, emphasizing the significance of the smooth signal term in achieving high classification accuracy.

G Additional Details on the Experimental Study

Reproducibility Statement

We ensure reproducibility by providing a detailed description of our methodology, including algorithmic steps (Algorithms 1, 2), evaluation procedures, and hyperparameter settings (Appendix G.3,G.2). The code used in this paper will be made available in a public repository upon acceptance. Full proofs of the theoretical results are included in the appendix, along with precise descriptions of our experimental setups.

G.1 Datasets Details

Table 7: Graph coarsening metrics experimental setting: Chosen hyperparameters for the Karate Club dataset at different coarsening ratios (r) and metrics.

Metric	Method	Karate Club dataset		
		$r = 0.7$	$r = 0.5$	$r = 0.3$
REE	INGC	β=0, λ=100, α=0.1	β=200, λ=10, α=1	β=100, λ=100, α=0.1
	SINGC	λ=0.1, α=0.1	λ=0.1, α=0.1	λ=0.1, α=0.1
RE	INGC	β=0, λ=1, α=200	β=200, λ=0.1, α=200	β=200, λ=1, α=200
	SINGC	λ=0.1, α=200	λ=0.1, α=200	λ=1, α=200
HE	INGC	β=0, λ=1, α=200	β=200, λ=0.1, α=200	β=200, λ=1, α=200
	SINGC	λ=0.1, α=200	λ=0.1, α=200	λ=10, α=200
DEE	INGC	β=0, λ=1, α=200	β=200, λ=1, α=200	β=0.1, λ=1, α=200
	SINGC	λ=10, α=200	λ=1, α=200	λ=200, α=200

Table 8: Graph coarsening metrics experimental setting: Chosen hyperparameters for the Les Miserables dataset at different coarsening ratios (r) and metrics.

Metric	Method	Les Miserables dataset		
		$r = 0.7$	$r = 0.5$	$r = 0.3$
REE	INGC	β=100, λ=200, α=0.1	β=200, λ=10, α=0.1	β=200, λ=200, α=1
	SINGC	λ=0.1, α=0.1	λ=100, α=0.1	λ=0.1, α=0.1
RE	INGC	β=200, λ=10, α=100	β=200, λ=10, α=200	β=200, λ=100, α=200
	SINGC	λ=0.1, α=100	λ=1, α=200	λ=100, α=100
HE	INGC	β=200, λ=10, α=100	β=200, λ=10, α=200	β=200, λ=100, α=200
	SINGC	λ=0.1, α=100	λ=0.1, α=200	λ=100, α=100
DEE	INGC	β=0, λ=200, α=200	β=0.1, λ=0.1, α=10	β=0.1, λ=0.1, α=200
	SINGC	λ=100, α=100	λ=10, α=100	λ=100, α=200

G.2 Node Classification Experiments Setting

The GCN model used in our experiments consists of two graph convolutional layers and is implemented using PyTorch and PyTorch Geometric libraries. The architecture is as follows:

- **Layer 1:** A Graph Convolutional Network (GCNConv) layer that takes the input node feature matrix X (with $X.shape[1]$ features) and outputs a hidden representation of size 64.
- **Layer 2:** A second GCNConv layer that maps the 64-dimensional hidden representation to the number of output classes (`NUM_OF_CLASSES`).

We use ReLU for non-linearity and dropout for regularization during training.

Table 9: Graph coarsening metrics experimental setting: Chosen hyperparameters for the Cora dataset at different coarsening ratios (r) and metrics.

Metric	Method	Cora dataset		
		$r = 0.7$	$r = 0.5$	$r = 0.3$
REE	INGC	β=10, λ=1, α=1	β=100, λ=1, α=1	β=200, λ=10, α=10
	SINGC	λ=1, α=10	λ=100, α=100	λ=200, α=0.1
RE	INGC	β=10, λ=100, α=200	β=100, λ=200, α=200	β=100, λ=10, α=200
	SINGC	λ=100, α=200	λ=0.1, α=100	λ=100, α=100
HE	INGC	β=10, λ=100, α=200	β=100, λ=200, α=200	β=100, λ=10, α=200
	SINGC	λ=100, α=200	λ=1, α=10	λ=100, α=100
DEE	INGC	β=0.1, λ=0.1, α=10	β=0.1, λ=100, α=200	β=0, λ=10, α=10
	SINGC	λ=100, α=200	λ=10, α=100	λ=100, α=200

Table 10: Graph coarsening metrics experimental setting: Chosen hyperparameters for the Citeseer dataset at different coarsening ratios (r) and metrics.

Metric	Method	Citeseer dataset		
		$r = 0.7$	$r = 0.5$	$r = 0.3$
REE	INGC	β=200, λ=200, α=200	β=100, λ=10, α=0.1	β=100, λ=10, α=0.1
	SINGC	λ=10, α=0.1	λ=100, α=0.1	λ=10, α=1
RE	INGC	β=100, λ=10, α=200	β=100, λ=1, α=10	β=0, λ=10, α=0.1
	SINGC	λ=1, α=100	λ=10, α=100	λ=100, α=200
HE	INGC	β=100, λ=10, α=200	β=0.1, λ=100, α=200	β=200, λ=0.1, α=0.1
	SINGC	λ=1, α=100	λ=1, α=100	λ=100, α=200
DEE	INGC	β=1, λ=0.1, α=0.1	β=200, λ=1, α=10	β=0.1, λ=0.1, α=10
	SINGC	λ=100, α=200	λ=100, α=200	λ=100, α=100

For SINGC, we set $t_{\text{iter}} = 2000$ in all experiments, and for INGC, we set $t_{\text{iter}} = 20$ and $c_{\text{iter}} = 100$. Tables 12 and 11 present the hyperparameters of our methods for each experiment. The results for the three baseline methods presented in Table 2 are sourced from Kumar et al. [14].

We note that tuning the hyperparameters in our methods is crucial for achieving optimal performance. By reviewing some of the corresponding setting in Tables 10, 9 and 11 we can observe that good performance often aligns with low values of REE and INP in this application. Therefore, we recommend that practitioners first optimize the hyperparameters by minimizing REE and INP. Once optimized, the coarsened graph can be used in the GNN for training and evaluation, leading to improved classification accuracy.

The additional details of real datasets are as follows:

Table 11: Node classification experimental setting: Chosen hyperparameters for the Cora Citeseer dataset at different coarsening ratios (r) and metrics.

Dataset	Method	Node Classification Parameters - Medium datasets		
		$r = 0.3$	$r = 0.1$	$r = 0.05$
Cora	INGC	β=100, λ=100, α=10	β=1, λ=100, α=1	β=1, λ=100, α=100
	SINGC	λ=10, α=0.01	λ=1000, α=1	λ=1000, α=0.01
Citeseer	INGC	β=0, λ=100, α=10	β=10, λ=1000, α=1000	β=0, λ=20, α=10
	SINGC	λ=50, α=20	λ=300, α=100	λ=50, α=10

Table 12: Node classification experimental setting: Chosen hyperparameters for the Co-phy, Pubmed, Co-CS dataset at different coarsening ratios (r) and metrics.

Dataset	Method	Node Classification Parameters - Large datasets		
		$r = 0.05$	$r = 0.03$	$r = 0.01$
Co-phy	INGC	β=10, λ=10, α=0.01	β=10, λ=1000, α=0.01	β=10, λ=1000, α=100
	SINGC	λ=100, α=0.01	λ=10, α=1	λ=10, α=100
Pubmed	INGC	β=0, λ=1000, α=0.001	β=0.1, λ=100, α=10	β=0.1, λ=100, α=100
	SINGC	λ=1000, α=0.001	λ=100, α=0.1	λ=10, α=10
Co-CS	INGC	β=1, λ=1000, α=10	β=0.1, λ=1, α=10	β=10, λ=100, α=100
	SINGC	λ=40, α=10	λ=10, α=10	λ=100, α=100

- **Karate Club** - $n = 34$, $p = 30$, $|\mathcal{E}| = 78$ - Here, nodes represent members of a karate club, and edges represent friendships between them. Synthetic features generated using the signal model presented at Section 3.1.
- **Les Miserables** - $n = 77$, $p = 50$, $|\mathcal{E}| = 254$ - Nodes represent characters in the novel *Les Miserables*, and edges indicate co-occurrence in the same chapter. Synthetic features generated using the signal model presented at Section 3.1.
- **Cora** - $n = 2,708$, $p = 1,433$, $|\mathcal{E}| = 5,429$ - Nodes represent research papers, and edges represent citation links between them. Node features correspond to the presence of specific words in each paper, and class labels indicate the paper's research field. Number of classes = 7.
- **Citeseer** - $n = 3,327$, $p = 3,703$, $|\mathcal{E}| = 4,732$ - Nodes represent research papers, and edges represent citation relationships. Node features are based on word occurrences in each paper, and class labels indicate the paper's topic. Number of classes = 6.
- **Co-Physics** - $n = 34,493$, $p = 8,415$, $|\mathcal{E}| = 247,962$ - Nodes represent physics research papers, and edges represent citations. Node features represent article keywords, and class labels indicate different fields of physics. Number of classes = 5.
- **PubMed** - $n = 19,717$, $p = 500$, $|\mathcal{E}| = 44,338$ - Nodes represent biomedical research papers, and edges represent citations. Node features are derived from TF-IDF scores of medical terms, and class labels indicate disease categories. Number of classes = 3.
- **Co-Computer** - $n = 13,752$, $p = 767$, $|\mathcal{E}| = 245,861$ - Nodes represent products in a co-purchase network, and edges indicate products frequently purchased together. Node features describe product attributes, and class labels represent product categories. Number of classes = 10.
- **Co-CS** - $n = 18,333$, $p = 7005$, $|\mathcal{E}| = 163,788$ - Here, nodes are authors, that are connected by an edge if they co-authored a paper; node features represent paper keywords for each author's papers, and class labels indicate most active fields of study for each author. Number of classes = 15.

G.3 Graph Coarsening Metrics Experiments Setting

Tables 7, 8, 9, and 10 present the hyperparameters of our methods for each experiment. For SINGC, we set $t_{\text{iter}} = 2000$ in all experiments, and for INGC, we set $t_{\text{iter}} = 20$ and $c_{\text{iter}} = 100$.

Regarding the implementation of the baseline comparison methods, the FGC hyperparameters were selected based on their optimal values as reported in their paper. The LVN and LVE methods were implemented using their provided graph coarsening libraries, with the maximum value of the parameter $K = k = r \cdot n$.

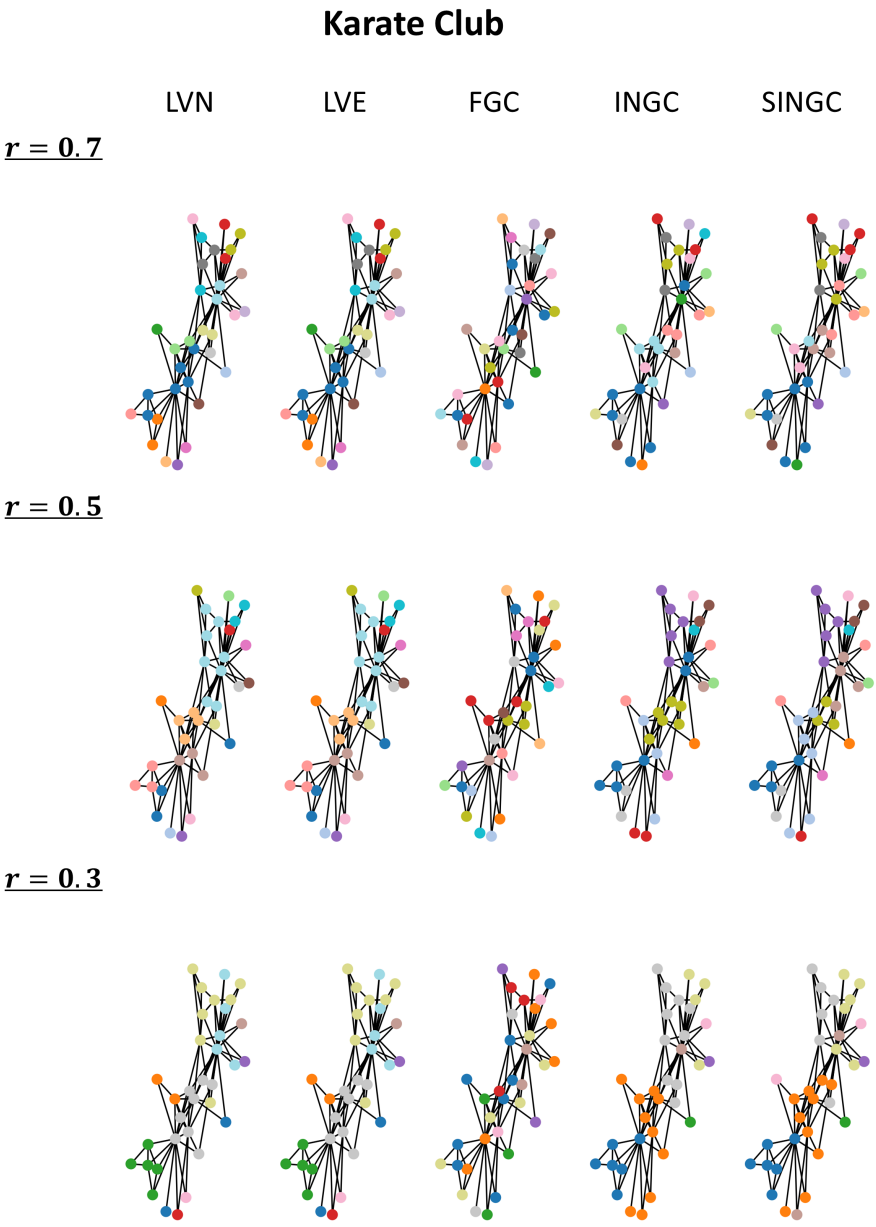

Figure 5: Visual comparison of coarsening methods on the Karate Club dataset. Each row displays the partitioning produced by each method at a different coarsening ratio. Nodes of the same color are grouped into the same super-node.

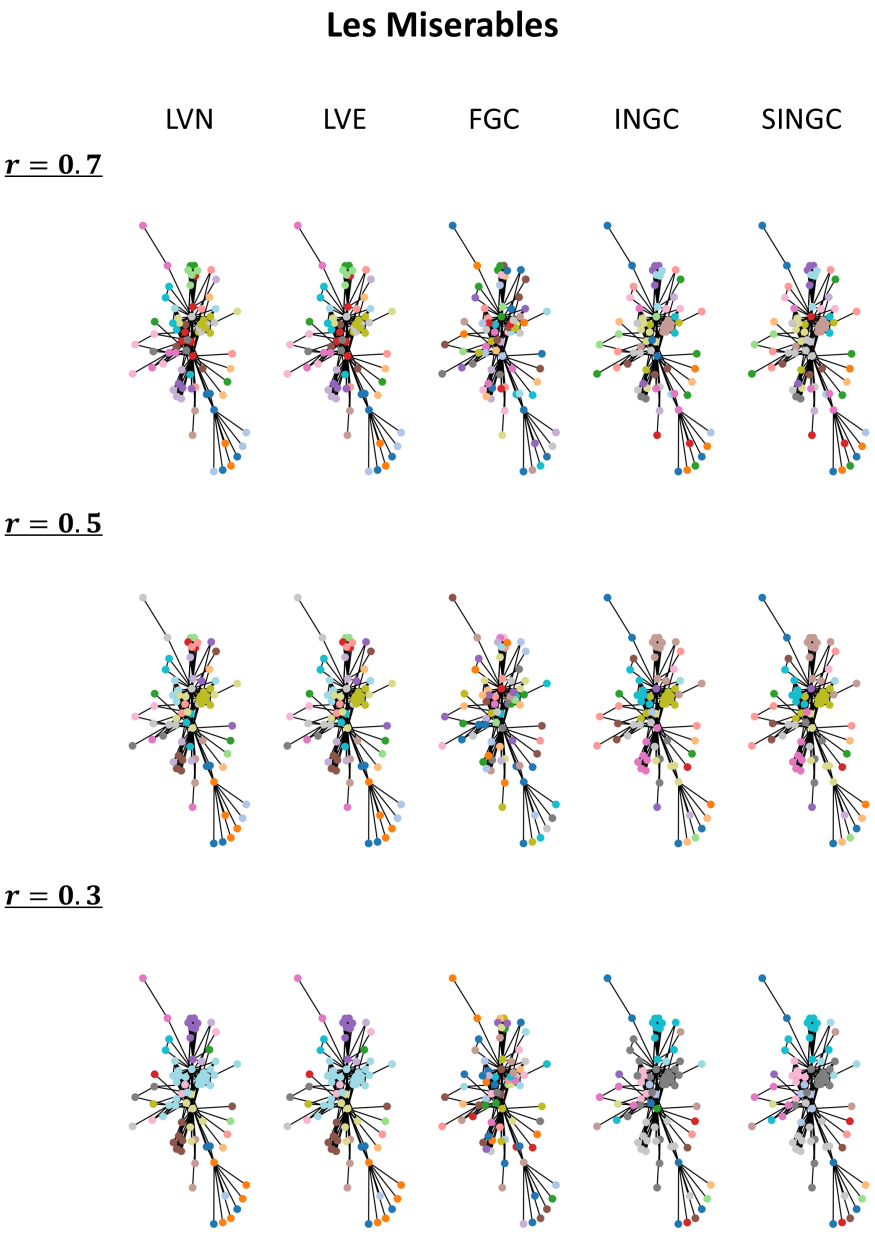

Figure 6: Visual comparison of coarsening methods on the Les Miserables dataset. Each row displays the partitioning produced by each method at a different coarsening ratio. Nodes of the same color are grouped into the same super-node.

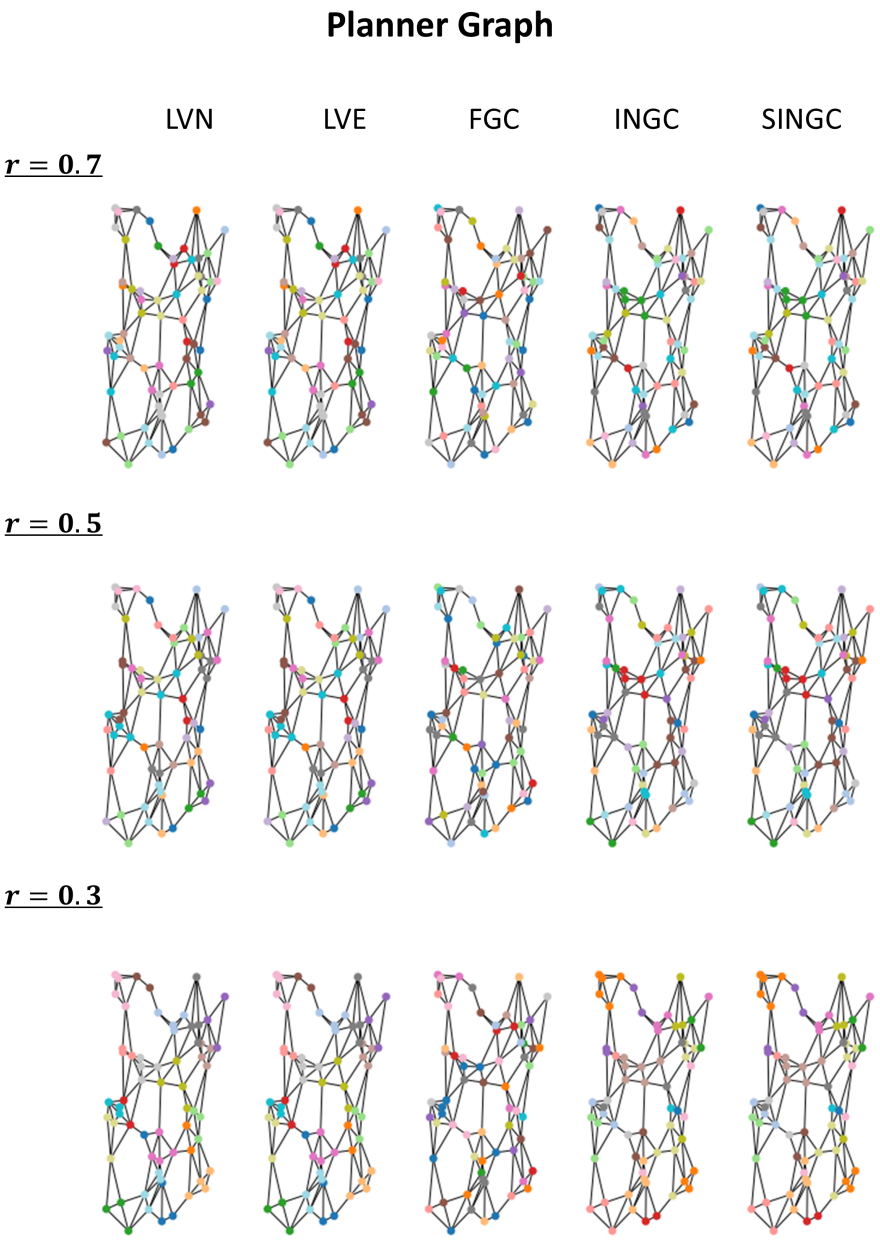

Figure 7: Visual comparison of coarsening methods on a planner graph. Each row displays the partitioning produced by each method at a different coarsening ratio. Nodes of the same color are grouped into the same super-node.